Computational and Structural Biotechnology Journal 21 (2023) 4336–4353

Contents lists available at ScienceDirect

Computational and Structural Biotechnology Journal

journal homepage: www.elsevier.com/locate/csbj

Research article

The World of GPCR dimers – Mapping dopamine receptor D_2 homodimers in different activation states and configuration arrangements

Beatriz Bueschbell [a,b], Pedro R. Magalhães [c], Carlos A.V. Barreto [a,b], Rita Melo [a,d], Anke C. Schiedel [e], Miguel Machuqueiro [c], Irina S. Moreira [f,g,*]

[a] CIBB - Center for Innovative Biomedicine and Biotechnology, University of Coimbra, 3000-456 Coimbra, Portugal
[b] IIIs-Institute for Interdisciplinary Research, University of Coimbra, 3000-456 Coimbra, Portugal
[c] BioISI - Biosystems & Integrative Sciences Institute, Faculty of Sciences, University of Lisboa, Campo Grande C8 bdg, 1749-016 Lisboa, Portugal
[d] Centro de Ciências e Tecnologias Nucleares, Instituto Superior Técnico, University of Coimbra, Coimbra, Portugal
[e] Department of Pharmaceutical & Medicinal Chemistry, Pharmaceutical Institute, University of Bonn, D-53121 Bonn, Germany
[f] Department of Life Sciences, University of Coimbra, Calçada Martim de Freitas, 3000-456 Coimbra, Portugal
[g] CNC-Center for Neuroscience and Cell Biology, CIBB-Center for Innovative Biomedicine and Biotechnology, University of Coimbra, 3004-535 Coimbra, Portugal

ARTICLE INFO

Keywords:
G protein-coupled receptor (GPCRs)
Dopamine receptor D_2
Homodimers
Dimer interface
Crosstalk
Selectivity

ABSTRACT

G protein-coupled receptors (GPCRs) are known to dimerize, but the molecular and structural basis of GPCR dimers is not well understood. In this study, we developed a computational framework to generate models of symmetric and asymmetric GPCR dimers using different monomer activation states and identified their most likely interfaces with molecular details. We chose the dopamine receptor D_2 (D_2R) homodimer as a case study because of its biological relevance and the availability of structural information. Our results showed that transmembrane domains 4 and 5 (TM4 and TM5) are mostly found at the dimer interface of the D_2R dimer and that these interfaces have a subset of key residues that are mostly nonpolar from TM4 and TM5, which was in line with experimental studies. In addition, TM2 and TM3 appear to be relevant for D_2R dimers. In some cases, the inactive configuration is unaffected by the partnered protomer, whereas in others, the active protomer adopts the properties of an inactive receptor. Additionally, the β-arrestin configuration displayed the properties of an active receptor in the absence of an agonist, suggesting that a switch to another meta-state during dimerization occurred. Our findings are consistent with the experimental data, and this method can be adapted to study heterodimers and potentially extended to include additional proteins such as G proteins or β-arrestins. In summary, this approach provides insight into the impact of the conformational status of partnered protomers on the overall quaternary GPCR macromolecular structure and dynamics.

1. Introduction

The G protein-coupled receptor (GPCR) family, the largest class of membrane receptors, targets more than 40% of the marketed pharmaceuticals [1]. Moreover, GPCRs mediate almost all (patho)physiological responses in humans [2,3]. Over the past few decades, it has been widely accepted that GPCRs increase their signaling repertoire by forming homo- or heterodimers, or even higher-order oligomers [4,5]. The physiological consequences of GPCR dimerization have been reported to modulate downstream signaling, trafficking, and regulation as well as the negative and positive cooperativity of ligand binding [6–8]. Dimerization can influence ligand recognition by modulating orthosteric and allosteric binding sites. It can also influence G protein-coupling and selectivity and may cause switching from G protein- to β-Arrestin-coupling [9]. Moreover, dimerization may lead to the formation of novel allosteric sites, resulting in different pharmacological properties [9].

Several GPCR dimers have been implicated in numerous pathological conditions, [6,10] including asthma, cardiac failure, preeclampsia, schizophrenia, and Parkinson's disease (PD), [6,10,11] which have drawn special interest in elucidating the mechanism of dimerization and oligomerization, as well as in the development of drugs that are capable of targeting both monomers within the dimers, known as bivalent ligands [4,6,8,12,13].

* Corresponding author at: Department of Life Sciences, University of Coimbra, Calçada Martim de Freitas, 3000-456 Coimbra, Portugal.
E-mail address: irina.moreira@cnc.uc.pt (I.S. Moreira).

https://doi.org/10.1016/j.csbj.2023.08.032
Received 25 April 2023; Received in revised form 29 August 2023; Accepted 29 August 2023
Available online 3 September 2023

In general, for class A receptors, transmembrane helices (TM) 1, 4, and 5 possess the largest membrane-accessible areas and hence have been reported to be of most relevance for dimerization [14]. It has been reported that the common orientations in class A dimers derived from crystal structures are head-to-head TM1/2 and TM4/5 [14]. Since most crystallographic structures miss the N- and C-termini and long intracellular loop (ICL) 3, these receptors and their possible roles cannot be clearly evaluated [15]. GPCR dimers have been shown to be possible in various *in vitro* studies. For instance, early studies by Guo et al. (2003, 2005, 2008) used cysteine-crosslinking and mutagenesis experiments with substituted cysteine residues [16–18]. Using cysteines to determine interaction contacts between proteins is advantageous for GPCRs, as cysteines are conserved in most rhodopsin-like GPCRs [19]. Cysteine contains a highly reactive thiol group, and a disulfide bond can be formed between two that are in close proximity under oxidizing conditions, which can only be reversed by reducing agents [20]. Furthermore, fluorescence/bioluminescence resonance energy transfer (FRET, BRET), time-resolved FRET strategies, and co-immunoprecipitation (Co-IP) have been increasingly successful in determining GPCR interfaces among other methods [8,21,22].

While classical biochemical methods, such as Co-IP, rarely determine the existence of such dimers and often require the availability of highly selective antibodies, RET methods are able to monitor their active movement [8]. For example, a study by Wouters et al. used complementation-based NanoLuciferase® Binary Technology (NanoBiT® assay) to investigate the effect of antagonists on the formation of D_2R-homodimers (D_{2long}), focusing on the TM5-TM6-TM5-TM6 interface [23]. Another recent study by Cheng et al. described a combinatorial approach using experimental and computational methods to characterize the interface of Apelin receptor (APJ)/Nociceptin receptor 1 (ORL1) and APJ/Vasopressin receptor 2 (V2R) dimers [22]. Chen and co-workers used a TM peptide containing a human immunodeficiency virus trans-acting transcriptional activator (HIV-TAT) protein transduction motif, together with matrix-assisted laser desorption tandem time-of-flight mass spectrometry (MADLITOF-MS) and BRET to demonstrate the switches of the dimers from active to inactive states [22]. They reported that transitions would range from a TM1/TM2 interface in the inactive state to an active TM5 interface [22]. From the obtained experimental information, they constructed atomic-resolution models.

Despite the development of several strategies to investigate GPCR dimers and probe their functional importance, a lack of resolution remains. While certain experimental approaches yield less-than-robust outcomes, computational calculations are demanding and time intensive. As a result, we directed our efforts toward the development of an easy-to-implement computational approach for a well-studied example of a GPCR dimer, the D_2R-homodimer, initially elucidated by Ng et al. in 1996 and recognized as having pathological relevance [24].

The five dopamine receptors (D_1R-D_5R) mediate the essential functions of dopamine and are highly promiscuous, forming homo- and heterodimers, as well as higher-order complexes that play a role in several neurological or neurodegenerative diseases [4,8,13,25–29]. By binding to different types of G proteins, the secondary messenger cAMP is stimulated or inhibited by dopamine receptors. D_1R and D_5R are coupled to $G\alpha_{s\ and\ olf}$ and are therefore classified as D_1-like receptors, whereas D_2R-D_4R is coupled to $G\alpha_{i/o}$ and belongs to D_2-like receptors [25,30,31]. In addition, D_2R exists in two isoforms, D_{2long} and D_{2short}, generated by alternative splicing [32]. Dimerization phenomena with their family members have been documented for all five receptors (D_1R-D_3R [33], D_1R-D_2R [34], D_2R-D_3R [35], D_3R-D_3R [36], D_2R-D_5R [37], D_4R-D_4R [38]; additional combinations are reviewed in Schiedel et al. [8,23,39]). Increased formation of the D_2R homodimer has been correlated with schizophrenia, chronic social defeat stress, and a sensitized state after amphetamine exposure, which can cause psychosis [23,40,41].

Although DR dimers have been analyzed in vivo and in vitro and the targetability of the dimers has been shown experimentally, the structural details are not yet fully understood. The crystal structure of GPCRs is a useful and indispensable tool for drug design [42]. However, *in silico* studies of GPCR dimers are scarce [43–45], with the dimer interface and monomer conformational states being unexplored for most known GPCR dimers.

Several studies by Guo et al. proposed a symmetrical interface of the D_2R homodimer involving TM4 [16–18]. This hypothesis was further supported by the existence of an interface between TM4 and TM5 in the inactive inverse agonist-bound state, whereas in the active state, TM4-TM4 was shown to form the interface [17]. In addition, a different study by Guo et al. identified a second symmetrical interface of TM1 that is relevant for higher-order oligomerization and does not seem to undergo major conformational changes upon ligand binding [18]. The authors showed that neither agonists (quinpirole and bromocriptine) nor antagonists (sulpiride and butaclamol) affected dimer formation and concluded that D_2R exists as a constitutive dimer [16]. Similar conclusions were drawn in a study by Armstrong and Strange, where radioligand binding studies using Chinese hamster ovary (CHO) cells showed that the D_2R homodimer has two identical and functional ligand-binding sites [46]. Moreover, receptor crosslinking, as observed by Guo et al., does not impair the inhibition of adenylate cyclase by dopamine [16–18]. Guo and coworkers concluded from their results that each of the D_2R dimer subunits is, therefore, able to bind to a G_i protein [16]. Using the same experimental approach, a similar pattern was found for the metabotropic glutamate 2 receptor ($mGlu_2R$) [47]. Both D_2R and $mGlu_2R$ homodimers share similar inactive interfaces via TM4-TM5, while the active interface occurs via TM4 in D_2R and via TM6 in $mGlu_2R$ [14]. Lee et al. studied the role of highly conserved cysteine residues in extracellular loops (ECL) 1 and 2 in D_2R oligomerization [19]. These cysteine residues are conserved in most rhodopsin-like GPCRs [19]. Cys→Ala mutations in the extracellular loops were not significantly different between mutant and wild-type D_2R. They also identified TM4 as the site of interaction in D_2R dimerization, which supports the proposal of a symmetrical TM4-TM4 interface. Like the full-length receptor, D_2R truncation mutants incorporating TM4 and TM5 (e.g., D_2TM4-ICL3) or consisting of TM1-TM4 (D_2AT-TM4) were able to form dimers. Truncated mutants lacking TM4 were identified as the monomers. To confirm this hypothesis, disruption of the helical structure of TM4 by the introduction of a proline residue in the truncation mutant, composed only of the TM4 and TM5 domains, prevented the formation of dimers. This is important evidence but does not exclude the possible role of TM5 in the dimerization process [19]. Marsago et al. showed another possible homodimer interface involving TM1 and TM2, along with HX8 [48]. In addition to these interfaces, it has been widely reported that D_2R can form heteromers through a TM4–TM5–TM4–TM5 interface with other class A GPCRs such as $A_{2A}R$ and angiotensin 1 receptors (AT_1R) [23]. However, such interfaces between homo- and heterodimers for the same GPCRs could be different [23]. More information on dimerization can be found in the Supplementary Information.

To date, the most biologically relevant interface for D_2R homodimers remains unclear. It is also possible that the interface depends on the specific conformation (active or inactive) of the protomers. According to Cordomi et al., activation of a single monomer implies a symmetry change in the established interface [14]. This was shown by Guo et al., where upon ligand binding, the D_2R homodimer interface moved from inactive TM4-TM5-TM4-TM5 toward an active TM4-TM4 interface [17]. Understanding the mechanism of action of D_2R homodimer formation as well as the interactions formed upon dimerization is of great importance and may offer new insights into the pathophysiology of dopamine-related diseases.

Hence, we delved into subsequent pivotal inquiries concerning interface composition and reorganization through examination of a prominent GPCR dimer illustration: (i) What conceivable configurations exist for the D2R homodimer?; (ii) Does the dimer configuration hinge on the activation state of monomers?; (iii) Do these configurations

exhibit physiological stability?; (iv) Which amino acids at the interface contribute to this process, along with their primary interactions?; (v) What specific structural and dynamic ramifications accompany dimer formation within the macroswitches and microswitches? We used published structures of D_2R in different conformational states: inactive (PDB-id:6CM4 [49]) and active (PDB-id:6VMS [50]). We successfully built several dimer models, studied them using molecular dynamics (MD) simulations, and performed a thorough structural analysis of the data.

2. Material and Methods

2.1. Homology modeling

The receptors were modeled using the MODELLER package [51] as previously described [52]. As stated in Preto et al. an Ala_n linker was added to connect TM5 and TM6, which were modeled with an extended helical segment (beyond the membrane) up to the linker, making the intracellular extension of these helices similar to that observed in the crystal structure of the β_2-adrenergic receptor (β_2AR)-Gs complex (PDB-id: 3SN6 [53]) and therefore corresponds to the D_{2short} isoform [52]. D_2R was modeled in three different conformations. The D_2R inactive (**in**) was based on the structure of the D_2R bound to risperidone (PDB-id: 6CM4 [49]), whereas the D_2R active (**ac**) (G protein-bound) was based on the D_2R-G protein complex (PDB-id: 6VMS [50]). The D_2R β-arrestin-bound conformation (**ar**) was modeled using the M2 muscarinic acetylcholine receptor (M_2R)-β-arrestin-complex (PDB-id: 6U1N [54]) as a template.

2.2. Dimer assembly protocol

The Kaczor et al. [15,27] pipeline was used to construct the D_2R homodimers. The protocol was applied for each configuration of the D_2R homodimer: inactive-inactive (6CM4–6CM4/**in-in**), two configurations of the active-active (6VMS-6VMS/**ac-ac** and 6VMS-6VMS-B/**ac-ac-B**, as a result of consensus scoring), arrestin-arrestin (6U1N-6U1N/**ar-ar**), active-inactive (6VMS-6CM4/**ac-in**), inactive-arrestin (6CM4–6U1N/**in-ar**) and active-arrestin (6VMS-6U1N/**ac-ar**).

2.3. Initial set of dimers

The initial set of possible dimer interfaces (composed of 144 conformational arrangements) was obtained by rotating one monomer around another in 30° steps. This task was performed using the Visual Molecular Dynamics (VMD) tcl script [55] provided by Kaczor et al. [15,27].

2.4. Protein-protein docking using Rosetta

Protein-protein docking using Rosetta [56] was applied to obtain 10 models per interface, resulting in a total of 1440 models. The docking was run in "*refine only*" mode to generate dimers compatible with membrane integration (as suggested by Kaczor et al.) [15,27]. Additionally, all 1440 models were analyzed using the *InterfaceAnalyzer* implemented by Rosetta [56].

2.5. Scoring parameters and scoring procedure

In our study, we used scoring parameters similar to the default ones, as they were previously considered capable of reproducing interfaces from X-ray structure dimers [15]. We used the Rosetta interface score (I_sc), solvent-accessible area buried at the interface (dSASA, like interface area), free energy of binding (dG_ separated), energy of hydrogen bond interactions (hbond_E_fraction), and number of residues at the interface (nres_int). All scores were provided by *InterfaceAnalyzer* [56], except for the Rosetta Interface score (I_sc), which is a direct output of the protein-protein docking procedure [56]. The number of residues at the interface (nres_int) was additionally chosen, assuming that a relevant interface would have a higher number of stabilizing interactions and that different combinations of conformations would likely involve a varying number of residues.

Two methods of consensus scoring were used, as previously described [27]: (i) average scores of the 100 best-scored dimers concerning each interface, and (ii) frequencies of the interfaces among the 100 best-scoring dimers. Before consensus scoring, values were normalized between 0 and 1. These two scoring methods were chosen to avoid bias when using only one method, and the top-scoring model was found using both methods. Similar to Kaczor et al. [15], we set the most favorable value of a given scoring factor in the normalization process to 1 and subsequently adjusted the other values. For dG_separated and hbond_E_fraction, negative values were considered favorable, whereas for dSASA and nres_int, positive values were considered favorable. For I_sc, Rosetta documentation considers values from − 5 to − 10 as a good interface score (https://www.rosettacommons.org/docs/latest/application_documentation/docking/dockinG protocol). To obtain the most favorable value for performing subsequent scoring, the mean of all 1440 models with an I_sc within this range was calculated upon normalization. Scores closest to 1 (range, 1.2, and 0.9) were selected for further evaluation.

The best interface for each configuration of the D_2R homodimer was selected based on the ranking of each parameter (the top three were considered). After determining the interface, all models (of the pool of 1440 models) possessing this interface were ranked again. The top three models were considered for selection of the final model. These were submitted for a quality evaluation.

2.6. Quality evaluation of the final dimer

The chosen representative model for each configuration of the D_2R homodimer was analyzed using PRODIGY-CRYSTAL, a machine-learning algorithm trained to distinguish between biologically relevant complexes and crystallization artifacts [57–59]. PRODIGY [59–61] was used to estimate the binding affinity, dissociation constant, and listing of interfacial residues. Finally, the predicted residues of PRODIGY-CRYSTAL and PRODIGY-PROTEIN were compared to define dimer interfaces of the selected models. Selected dimers were inserted into a lipid bilayer system and subjected to MD simulations. To easily locate relevant residues and important motifs and compare them to other GPCRs, residues were annotated using the Ballesteros and Weinstein nomenclature [62]. According to this nomenclature, the first digit identifies the TM helix and the second digit identifies the residue position in relation to the most conserved residues on each helix (assigned index number X.50). Subsequently, the number decreases towards the N-terminus and increases towards the C-terminus [62,63].

2.7. Molecular dynamics simulations

2.7.1. Membrane orientation

Protein orientation in the membrane was obtained using the OPM-PPM-server for every modeled dimer structure (https://opm.phar.umich.edu/ppm_server) [64].

2.7.2. System building

The dimer structures (as well as the monomers to be used as controls) were inserted into a lipid bilayer membrane in a cubic simulation box hydrated with TIP3 waters and 0.15 M NaCl using CHARMM-GUI Membrane Builder (http://www.charmm-gui.org) [65–68]. Termini ACE (or ACP in the case of the D_2R **ac-monomer**)/CT1 were used as caps at the N- and C-termini. Disulfide bonds were established between residues 79/154 and 249/251 in the **in-monomer** and **ar-monomer** structures, respectively. As the template structure of the **ac-monomer** (6VMS) was found to be three amino acids shorter at the N-terminus,

their disulfide bonds involved residues 76/151 and 246/248. Palmitoylation of the last Cys residue (Cys293 for **the in-monomer**, **ar-monomer**, or Cys290 for **the ac-monomer**) was performed. The protonation state of the important Asp at position 2.50 was defined as follows: for the D_2R **in-monomer,** it was charged (not protonated), whereas for the D_2R **ar-monomer** (residue 52) and **ac-monomer** (residue 49), it was set to neutral (protonated), as upon class A GPCR activation, protonation of $Asp^{2.50}$ takes place due to dehydration and displacement of the $Asp^{2.50}$-bound sodium ion [69–73]. Owing to the importance of water molecules for GPCR activation, [69] we also added pore water using protein geometry. A heterogeneous lipid bilayer was built around the dimer structures with POPC and cholesterol (CHL1) (ratio 9:1), with 240 lipids in each leaflet (for the monomers, 100 lipids per leaflet were chosen). The size of the x/y plane is based on the number of lipid components. The box was rectangular, and its hydration number was set to 100 (100 water molecules per lipid). The D_2R **ac-monomer** (single and part of the dimer) also contains the co-crystallized ligand bromocriptine in the same orientation as the 6VMS crystal structure (PDB-id:6VMS [50]). Consequently, the **ac-ac** dimer possesses two ligands, one per receptor. The ligand itself was parameterized using the CHARMM-GUI ligand reader and modeller [74], and added to the system while building CHARMM-GUI. CHARMM36m was selected as the force field [66]. The remaining options were set to their default values.

2.7.3. Molecular dynamics parameters

MD simulations were performed using GROMACS 2019.4 and the CHARMM36m force field [66,75–77]. The systems were simulated using the NPT (isothermal-isobaric) ensemble. To achieve and maintain the desired temperature (310 K), a v-rescale thermostat was used, with a coupling constant of 0.1 ps [78]. Pressure coupling was performed using a semi-isotropic Parrinello-Rahman barostat at 1 bar with a compressibility of 4.5×10^{-5} bar^{-1} and a coupling constant of 1.0 ps [79,80]. Electrostatic interactions were computed with the particle-mesh Ewald (PME) method with a Fourier grid of 0.12 nm and a cut-off of 1.2 nm for direct contributions [81,82]. Lennard-Jones interactions were computed using a non-bonded neighbor pair list with a cut-off of 1.2 nm, enabling the use of the Verlet scheme [83]. Solute bonds were constrained using the Parallel LINear Constraint Solver, P-LINCS [84]. The steepest descent algorithm was used to minimize the initial energy of the system through a 50,000-step run [85]. The systems were then initialized for 25 ns: five runs of 5 ns each with successively lower constraints for lipid heavy atoms and protein carbon alpha (1.000, 500, 100, 10, and 0 kJ nm^{-2} mol^{-1}). Three replicates (500 ns long) were performed for each dimer configuration and monomer, and the initial 200 ns were discarded to ensure a good system equilibration.

2.8. Analysis

Plots were generated using GraphPad Prism (GraphPad Prism Version 8.1.0, GraphPad Software, San Diego, California, USA, www.graphpad.com) and Gnuplot (Gnuplot Version 5.2, Williams, T., and Kelley, C., www.gnuplot.info). Residue-residue interactions were determined using GetContacts (https://getcontacts.github.io/interactions.html), and flare plots were created using gpcrviz.github.io/flareplot/?p = create. All the remaining calculations were performed using in-house scripting.

We focused our analyses on the transmembrane helices, loops, and structural motifs, including DRY ($Asp^{3.49}$, $Arg^{3.50}$, and $Tyr^{3.51}$), CWxP ($Cys^{6.47}$, $Trp^{6.48}$, $Leu^{6.49}$, and $Pro^{6.50}$), ionic lock ($Arg^{3.50}$ and $Glu^{6.30}$), NPxxY ($Asn^{7.49}$, $Pro^{7.50}$, $Ile^{7.51}$, $Ile^{7.52}$, and $Tyr^{7.53}$), PIF ($Pro^{5.50}$, $Ile^{3.40}$ and $Phe^{6.44}$), arginine cage ($Ile^{3.46}$ and $Leu^{6.37}$), serine microdomain ($Ser^{5.42}$, $Ser^{5.43}$,and $Ser^{5.46}$), and rotamer toggle switch ($Trp^{6.48}$, $Phe^{6.51}$, $Phe^{6.52}$, and $His^{6.55}$), which were previously described as important determinants of the GPCR activation mechanism [63,86,87]. The following calculations were performed: (i.) the distance over time between a subset of residues located roughly at the center of each TM and the average position of the membrane using its phosphorus atoms as references; (ii.) the root-mean-square-deviation (RMSD) of the TM and the other mentioned domains; (iii.) the relative dimer orientation by calculating two pseudo-dihedral angles along the MD simulations: θ1 consisting of residues $Phe^{1.48}$, $Ser^{4.53}$, $Ile^{4.56}$ from protomer 1 and $Ile^{4.56}$ from protomer 2; and θ2, consisting of residues $Phe^{1.48}$, $Ser^{4.53}$, $Ile^{4.56}$ from protomer 2 and $Ile^{4.56}$ from protomer 1; (iv.) the solvent-accessible surface area (SASA); (v.) the number of intermolecular H- bonds, salt bridges, π-cation, π-stacking and T-stacking interactions using GetContacts; (vii.) pairwise distances between Cα-Cα of interfacial residues; (viii.) TM5 bulge as the distance between the heavy atoms of $Ser^{5.46}$ and $Leu^{7.41}$; (ix.) ΔRMSD as the difference between the average RMSD of $Ile^{3.40}$ and $Phe^{6.44}$ heavy atoms and the inactive and active structures 2RH1 [88] and 3P0G [89], respectively; (x.) angles between the centroids of the benzene ring of three phenylalanines $Phe^{5.51}$, $Phe^{6.44}$ and $Phe^{6.45}$ over time; (xi.) distance between the Cα atom of $Asp^{2.50}$ and the closest sodium atom; (xii.) number of water molecules within an 8 Å distance cut-off of $Asp^{2.50}$; (xiii.) the angles between the Cγ atom of $Lys^{3.43}$, the Cβ atom of $Val^{6.41}$, and the Cβ atom of $Ile^{6.40}$; (xiv.) RMSD of the NPxxY domain and the distance between Cα atoms of residues of the ionic lock, $Arg^{3.50}$ and $Glu^{6.30}$; (xv.) size of the binding sites for the G protein and β-arrestin using the SASA values of relevant residues and normalized to the $SASA_{max}$ values determined earlier for each type of amino acid.

3. Results

3.1. Model generation and analysis

The application of typical protein-protein docking procedures to GPCR dimers is not straightforward [90,91]. A previously published protocol has been successfully applied to model a D_2R homodimer in an inactive conformation [15,27], among other studies of different GPCRs [92,93]. Therefore, we have extended its application to other possible configurations of D_2R homodimers in various activation states. After selecting the most suitable models for MD simulations, they were checked for overall structural equilibration over time. Next, the interface and relevant residues were identified and compared with the initial prediction before the structural relaxation was obtained using MD simulations. Important macro- and microswitches for class A GPCR activation were analyzed and compared among dimer configurations to observe any conformational changes in the monomers when complexed as dimers (protomers). Significant interfacial elements were assessed and compared.

3.2. Contributing transmembrane helices

Upon generation of dimer models, it was shown that different combinations of TMs were involved in the establishment of the interface (Table 1, Fig. S1). To determine the biological relevance of our different D_2R decoy configurations, they were subjected to PRODIGY-CRYSTAL and PRODIGY-PROTEIN algorithms (Table S1). Using consensus scoring, we selected two **ac-ac** dimers as equally possible: one with the

Table 1
The proposed interfaces for the D_2R homodimer configurations were based on consensus scoring (Fig. S1).

	Dimer configuration	Proposed interface	Template used
1	in-in	TM4-TM5-TM4-TM5	6CM4–6CM4
2	ac-ac-B	TM4-TM5-TM7-TM1	6VMS-6VMS-B
3	ac-ac	TM4-TM5-TM4-TM5	6VMS-6VMS
4	ar-ar	TM4-TM5-TM4-TM5	6U1N-6U1N
5	ac-in	TM1-TM2-TM4-TM5	6VMS-6CM4
6	in-ar	TM3-TM4-TM4-TM5	6CM4–6U1N
7	ac-ar	TM4-TM5-TM4-TM5	6VMS-6U1N

proposed TM4-TM5-TM4-TM5 interface and a second (B) with a proposed TM4-TM5-TM7-TM1 interface (Table 1, Fig. S1).

The TM4-TM5-TM4-TM5 interface was the most prominent among the dimers. Other possible interfaces were determined for the **ac-ac-B**, **ac-in,** and **in-ar** dimers. For D_2R, only **in-in**, **ac-ac**, and **ac-in** D_2R homodimers have been experimentally detected; however, other combinations are also possible [17,94,95].

3.3. Predicted interface in models

We identified interfacial amino acids in the static model structures using both PRODIGY algorithms (Table S2) [57–59]. We found that the number of residues varied between 21 and 35 and that the composition of interfacial amino acids was slightly different among the different D_2R homodimer configurations. Although the total number of interfacial amino acids differed between dimer configurations, they were similar for pairs of monomers complexed together (Table S2). In addition, we identified amino acids present in two or more dimers, marked in bold in Table S2, whereas the others were unique (frequency = 1), marked in italics in Table S2. Subsets of frequently appearing amino acids were found in configurations with a symmetric interface (TM4-TM5-TM4-TM5). No unique residues were found for one protomer in the **in-in**, **ar-ar**, or **ac-protomer** of the **ac-ar** configuration. We also analyzed the frequency of common residues across all dimer configurations (Table S3). The 98 residues were sorted into three categories: very frequent (8–12x), moderate (3–7x), and rare (1–2x). Nineteen frequent residues were found: 110Met (ICL2), 160Ala (ECL2), $Tyr^{3.48}$, $Tyr^{3.51}$, $Thr^{3.52}$, $Ala^{3.55}$, $Arg^{4.40}$, $Arg^{4.41}$, $Val^{4.44}$, $Ile^{4.48}$, $Leu^{4.52}$, $Thr^{4.55}$, $Pro^{4.59}$, $Tyr^{5.41}$, $Val^{5.45}$, $Val^{5.49}$, $Ile^{5.52}$, $Val^{5.53}$, and $Leu^{5.56}$. More detailed analyses of the various interfaces are provided in Supplementary Information.

3.4. Analysis of the simulated systems

After analyzing the final models, they were subjected to MD simulations. We first ensured that the systems were stable during the simulation, that is, no disruption of the dimer occurred, and that the binding interfaces achieved equilibrium before further analysis. This was the case for all models except for **ac-ac-B**, which was disrupted upon initialization and excluded from further analysis (Fig. S2).

3.5. Equilibration and stability of the systems

The equilibration of the system was evaluated by calculating the distance over time between a subset of residues located approximately at the center of each TM and the average position of the membrane P atoms. Two residues were selected per TM (1.44, 1.45, 2.52, 2.53, 3.37, 3.38, 4.51, 4.52, 5.49, 5.50, 6.44, 6.45, 7.49, and 7.50), and their distance to the membrane center along the z-coordinate was calculated (Fig. S2). Based on these results, an equilibration period of 200 ns was determined to be appropriate (the black area in Figure. S2). RMSD calculations were used to determine the stability and relative orientation of the TMs, loops, and important structural motifs of the D_2R homodimer, and were compared with those of the monomers (Fig. S3). RMSD calculations were therefore performed for the individual monomers (in M), for each protomer within the dimer (in D), and for the entire dimer itself (Dim), and averaged among replicates. Overall, the systems were stable over time, with no major movement or disruption of TMs. Analysis of microswitches and key domains showed that dimers had higher RMSD values than monomers, likely due to conformational rearrangement upon complex formation. A more widespread distribution was also observed for dimers, particularly at the DRY, CWxP, NPxxY, PIF, arginine cage domains, serine residues, and toggle switch, likely because of the same conformational rearrangement. We also monitored certain macro- and microswitches over time, including the relative orientation of the dimers (Fig. S4), the interface area (Fig. S5), the distance between TM3-TM6 (Fig. S9) and TM3-TM7 (Fig. S10), the angle between the centroids of the benzene ring of residues 5.51Phe, 6.44Phe, and 6.45Ile (Fig. S18), the opening of the hydrophobic lock (Fig. S20), both angles χ_1 and χ_2 of $Tyr^{7.53}$ (Figs. S21 and S22), and the sizes of the G protein and β-arrestin binding sites (Figs. S28 and S29). For most time series analyses, no major changes were observed, indicating that an equilibration time of 200 ns was sufficient for the systems to converge.

3.6. The D_2R homodimer interface

3.6.1. Relative orientation of the dimers

The relative orientation of the receptors in the dimeric state was determined by calculating the relative rotational angles of the two receptors (Fig. S4). The two-dimensional plots indicate that the symmetrical **in-in** dimer was highly stable across the MD simulations, suggesting a nonflexible dimer interface. Except for the **ac-ac** configuration, all other configurations populated two similar conformation states. The **ac-ac** configuration showed higher plasticity and could be mapped to three different dimer configurations.

3.6.2. Key residues and interface area

We calculated the interface area values of various dimer configurations (Fig. 1 **and S5**) and found that these values were consistent across replicates over time. Regarding the size of the homodimer interface, the smallest area was observed in the **ar-ar** configuration, whereas the largest area was observed in the **in-ar** configuration. Furthermore, configurations with the same interface type (e.g., TM4-TM5-TM4-TM5) varied in size, with **ar-ar** configurations having the smallest interfacial area and **in-in** configurations having the largest interfacial area.

To consider the dynamical behavior of the systems and to determine which residues formed the so-called "decoy original interface" of the dimer, we calculated the ΔSASA of each residue at the start of the simulation, where $\Delta SASA = SASA_m - SASA_d$, where $SASA_m$ and $SASA_d$ are the SASA values in the monomeric and dimeric forms, respectively. The rationale was that residues with a ΔSASA of 0 had the same exposure in both dimeric and monomeric forms and, as such, were not part of the initial interface. In addition to the requirement of a $\Delta SASA > 0$, we employed another set of criteria to further narrow down this list: residues should have a ΔSASA higher than 0.05 nm^2 in at least 2 out of the 3 replicates. We then calculated ΔSASA over time for each residue on this list, and for each residue, we performed normalization by dividing it by $SASA_{max}$, defined as the maximum SASA value for that residue type (i.e., when fully exposed). Only residues with a normalized ΔSASA of > 10%

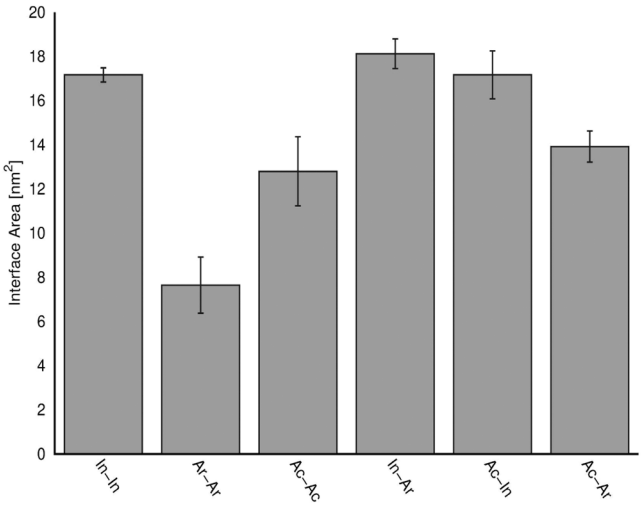

Fig. 1. Interface area of each D_2R homodimer system. The interface area was calculated for each system, and replicates are summarized as the mean ± standard error of the mean (SEM).

were considered to belong to the initial interface (Fig. S6, Table S4).

We observed that most of the residues of the original interface remained there for more than 50% of the simulation time; however, there were a few exceptions (a detailed analysis can be found in Fig. S6 and Table S4). In addition, we also found that a significant number of residues located in the loops contributed to the interface, especially residues from ICL2 (110Met, 111Pro, 112Met, 113Leu, 114Tyr, 115Asn, 116Thr, 117Arg, 118Tyr, 119Ser, 120Ser, 121Lys) and ECL2 (144Phe, 145Gly, 146Leu, 147Asn, 148Asn, 158Asn, 159Pro, 160Ala). In addition, we determined that TM7 and ICL3 do not contribute to the interface of any configuration. For **in-protomer-2** of the **in-in** dimer and **in-protomer** of the **in-ar**, but not for **the ac-in**, two residues from TM6 ($Ile^{6.56}$, $Ile^{6.59}$) were part of the interface, which was unexpected because TM6 was not part of the initially predicted interface. In addition, **ar-protomer-2** of the **ar-ar** configuration and the **in-protomer** of the **in-ar** configuration possessed 248His (ECL3) as part of their interface. For the two hetero-configuration dimers, **ac-in** and **in-ar**, residues from TM1, ICL1, and TM2 ($Val^{1.51}$, $Cys^{1.54}$, $Met^{1.55}$, $Ser^{1.58}$, $Arg^{1.59}$, 35Lys, 38Gln, $Tyr^{2.41}$, $Val^{2.48}$, $Leu^{2.52}$, $Thr^{2.55}$, and $Leu^{2.56}$) contributed to the interface. While the **ac-in** configuration was formed by TM1-TM2 of the **ac-protomer**, the **in-ar** configuration was formed by TM4-TM5 of the **ar-protomer**. A unique feature was also observed in the **ar-protomer** of the **in-ar** configuration, which contained one ECL1 residue (75Ser) and two HX8 residues ($Ile^{8.53}$ and $Cys^{8.56}$) at the interface.

We compared the "original decoy interface" with the prediction made with the PRODIGY/static structure using homodimers before they underwent MD simulations (Table S5) [57–59]. Although most residues were accurately predicted, there were some changes in the interface residue list, indicating some conformational rearrangements. Notably, all relevant residues from the Guo et al. study were present in all dimer configurations (Fig. 2) [16–18].

3.6.3. Predicted static interface vs. dynamical interface

After comparing the PRODIGY/static structure and SASA/dynamic interfaces and sorting all residues according to their frequency (Table S2-S6), we identified the following highly frequent residues in the D_2R homodimer:160Ala (ECL2), $Arg^{4.40}$, $Val^{4.44}$, $Ile^{4.48}$, $Val^{4.51}$, $Leu^{4.52}$, $Thr^{4.55}$, $Pro^{4.59}$, $Tyr^{5.41}$, $Val^{5.45}$, $Val^{5.49}$, and $Val^{5.53}$. Interestingly, we also observed that partnered protomers with different TMs, such as the **ac-protomer** of the **ac-in** configuration, which uses TM1 and TM2 as part of the interface, also included $Arg^{4.40}$ and $Val^{4.51}$ among the prevalent residues. Similarly, the **in-protomer** of the **in-ar** configuration, which uses TM3 and TM4 as part of the interface, contains residues from TM5 ($Val^{5.40}$, $Tyr^{5.41}$, $Ile^{5.44}$, $Val^{5.45}$, $Val^{5.49}$, $Ile^{5.52}$, $Val^{5.53}$, $Leu^{5.56}$, $Lys^{5.60}$, and $Arg^{5.67}$) and TM6 ($Arg^{6.67}$, $Ile^{6.56}$, and $Ile^{6.59}$).

In addition to the highly prevalent residues, certain regions of the receptor also contribute to the size of the interface in the dimer with the TM4-TM5-TM4-TM5 interface, such as TM3, ECL2, and ICL2. For example, many residues from TM3 and the loops contributed to the interface in the **in-in-symmetric** dimer, but this was not the case for the **ac-ac** and **ar-ar** dimers. Almost no residues from the loops contributed to the interface in the **ar-ar** homodimer. In contrast, various residues from the loops were important for binding in the **ac-ac** dimer, but only one residue from TM3 ($Ala^{3.55}$) was part of the interface. Similarly, only $Ile^{3.48}$ and $Thr^{3.52}$ were part of the TM4-TM5-TM4-TM5 interface in the **ac-ar configuration.**

For dimers with a nonsymmetric interface, such as **ac-in** (TM1-TM2-TM4-TM5), we again found that residues from other regions, such as TM3 and ICL1, contributed to the interface. Interestingly, for the **in-ar** (TM3-TM4-TM4-TM5) configuration, some residues from TM5 and TM6 were part of the interface on the **in-protomer** side (TM3 and TM4), while residues from TM1, ICL1, TM2, TM3, and HX8 contributed from the **ar-protomer** side (TM4-TM5). This finding was consistent with the large interfacial area of the **in-ar** configuration (Fig. 1). The same observation was made for the **ac-in** interface (Fig. 1).

In addition to the size of the interface area and, consequently, the number of interfacial residues, we also determined the types of residues that are preferentially conserved in these interfaces. As expected, most of the 12 conserved/highly frequent residues were nonpolar, including 5 valine residues. Asp and Glu were the only amino acid residues not found at any interface.

3.6.4. Interaction type established for the different interfaces

The type of pairwise interaction was determined and averaged among the replicates (Fig. S7). Each system displayed a unique pattern, and interestingly, they were not solely found between the TMs of the partnered receptors (a detailed analysis is shown in Fig. S7).

Overall, the results showed that the conformational states of the monomers contributed to the interaction patterns when considering dimer configurations with the same interface. For example, in the **in-in**

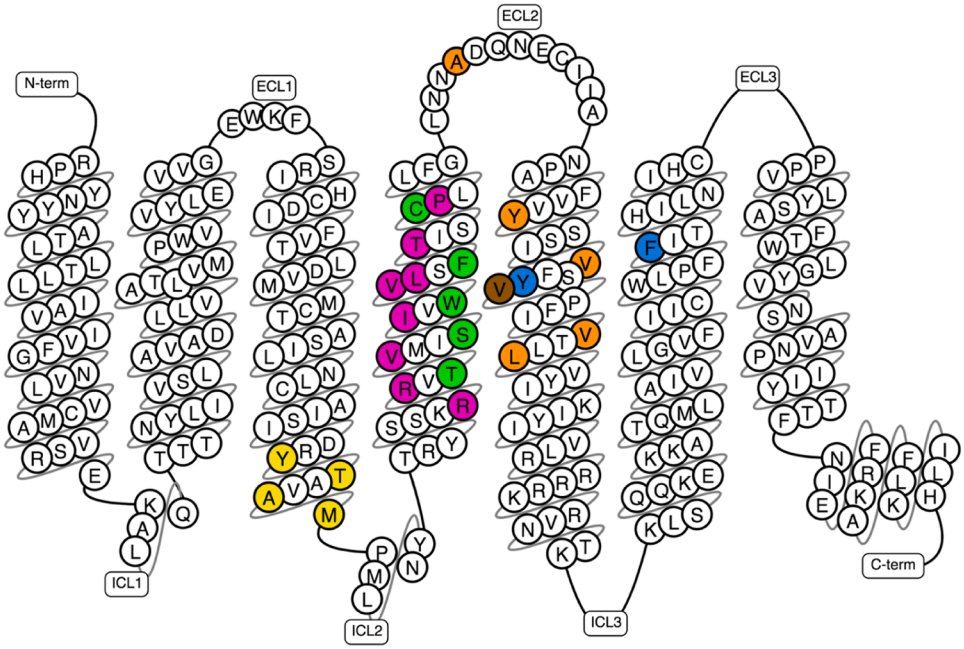

Fig. 2. Snake plots of relevant residues from the literature and this study. Residues found in the active conformation in the study by Guo et al. are shown in green [16–18]. The residues that are important for the interface between TM5 and TM6, as described by Wouters et al., are shown in blue. Residues shown in yellow were predicted in our study by PRODIGY, and residues in brown by SASA [23]. Residues predicted by both PRODIGY and SASA are shown in orange, and residues predicted in our study and those described by Guo et al. are shown in pink.

configuration, interactions involving TM5 were not present even though TM5 was part of the interface. TM4 was relevant for forming H-bonds and π-cation interactions with ICL2 as well as H-bonds and salt bridges with TM3. The subset of interfacial residues on TM3 comprises Ile$^{3.48}$, Tyr$^{3.51}$, Thr$^{3.52}$, and Ala$^{3.55}$. ICL2, ECL2, and ECL3 are domains mainly involved in the formation of π-stacking, T-stacking, and some H-bond and π-cation interactions, respectively. Moreover, residues from ECL3 have not previously been identified as part of the interface. ICL2 consisted of only a few residues that were involved in interface formation:110Met, 111Pro, and 120Ser, whereas the ECL2 interfacial residues were 146Leu, 147Asn, 159Pro, and 160Ala. Ile$^{6.59}$ was the only relevant residue identified in TM6.

When comparing these findings to those of other configurations with the same interface, we found that for **ar-ar** and **ac-ac,** no salt bridges were present. However, conserved salt bridges between TM4 and TM3 were found in the **ac-ar** configuration, similar to our observations for the **in-in** configuration. In the **ar-ar** configuration, TM4 and TM5 are involved in the formation of H-bonds. Although this configuration has the smallest interface (Fig. 1), with only 12 residues, it appears to be crucial for many interactions.

For instance, the TM5 residues, comprising Phe$^{5.38}$, Tyr$^{5.41}$, and Val$^{5.45}$ from protomers 1 and Val$^{5.40}$, Ile$^{5.44}$, Tyr$^{5.48}$, Val$^{5.49}$, Ile$^{5.52}$, Leu$^{5.56}$, Lys$^{5.60}$ from protomer 2. Only π-cation interactions are formed by residues TM4, ECL2, and ECL3. In contrast to the **ar-ar** and **in-in** configurations, the **ac-ac** configuration behaved differently. H-bond interactions were mainly formed by TM3, TM4, and TM5, while π- and T-stacking interactions were mostly formed by TM5. However, for this configuration, the loops appeared to be less involved in stabilizing the interactions. This was also true for the **ac-ar** configuration. We concluded that TM3 was highly involved in other types of interactions, such as H-bonds and π-cation interactions, which is quite interesting because only Ile$^{3.48}$ and Thr$^{3.52}$ were previously considered to be part of the interface. When examining the major structures involving mixed conformational dimers, such as **in-ar** and **ac-in**, a larger subset of salt bridges was found compared to other homo-conformational configurations. For the **in-ar** configuration, ICL1 residues 35Lys and 38Gln were also involved in the observed interactions. Interestingly, π-cation interactions were also formed by residues from HX8. For the **ac-in** configuration, HX8 also contributed to the H-bond and π-cation interactions. In this configuration, residues from TM1, TM2, TM4, and TM5 interacted with each other or with residues from the loops, particularly ICL2 (117Arg, 118Tyr, and 121Lys) and ECL2 (144Phe, 145Gly, 147Asn, and 160Ala).

3.7. Macro- and microswitches upon dimerization

The effects of activation on different macro- and microswitches are reviewed in the Supplementary Information. In this study, we investigated these effects in the context of dimerization.

3.7.1. Outward movement of TM6, inward movement of TM7, and disruption of the ionic lock

A description of the GPCR activation mechanism and its main effects can be found in Supplementary Information (Fig. S8). First, we compared the distance between the Cα atoms of residues 3.50–6.34 (TM3-TM6) and 3.50–7.53 (TM3-TM7) (Fig. S9 and S10). Arg$^{3.50}$ is part of the ionic lock and is known to form a salt bridge with Glu$^{6.30}$, stabilizing the inactive state [96–98]. The ionic lock was disrupted upon activation, leading to the outward movement of TM6, for which 6.34 was chosen as the representative part of the key DRY motif [99]. Tyr$^{7.53}$, also part of the NPxxY motif, is a highly conserved tyrosine that undergoes conformational transitions depending on the activation state of the receptor [96,100]. According to Zhou et al., Tyr$^{7.53}$ also experiences several rewiring events with a shortening of its distance to TM3 [87]. As expected, we obtained a shorter TM3-TM6 distance and a higher TM3-TM7 for the **in-monomer** conformation, whereas these values were higher for the **ar-** and **ac-monomers** and dimers containing them. For the various dimer configurations, we observed that the TM3-TM6 distances were (i) even lower for **in-in**, (ii.) lower for one protomer on the **ar-ar** dimer, (iii.) constant for the **ar-protomer** in **the in-ar** and **ac-ar;** (iv.) higher for the **ac-protomer** in the **ac-ar** dimer, and (v.) lower for the **ac-protomer** in the **ac-in** dimer configuration.

Second, the distances between the Cα atoms of residues 3.50 and 6.34 (TM3-TM6) and between 5.46 and 7.41 (TM5-TM7) were measured to observe the overall concerted movement of the TMs (Fig. S11, S12). The role of these residues in activation is further explained in the Supplementary Information. As for TM3-TM7 (3.50–7.53), the distance between TM5-TM7 (5.46–7.41) should also be short when the receptor is activated. For the distance between TM5 and TM7, we expected distances to be similar to those observed for TM3-TM7. When comparing these two measurements for the individual monomers, we found that the distance between TM3-TM6 was shorter (between 0.5 and 1.0 nm) for the **in-monomer**, while the distance between TM5-TM7 was larger (between 1.6 and 2.0 nm). For the **ar-monomer,** the distance between TM3-TM6 was consistent at approximately 1–1.5 nm, while a high dispersion was found for the TM5-TM7 distance ranging from 1.4 to 2.4 nm over time. However, the distance between TM5-TM7 is much larger than that between TM3-TM7. The opposite was true for the **ac-monomer** configuration. The distance between TM5 and TM7 was consistently between 1.6 and 2 nm over time, which was larger than the distance between TM3 and TM7. In contrast, the distance between TM3 and TM6 exhibited considerable variability over time, ranging from 0.7 to 1.7 nm.

As a third metric, we analyzed the distance between the Cα atoms of residues 3.50 and 6.34 and between 5.58 and 7.53 (Fig. S13, S14). The distance between 3.50 and 6.34 is an indicator of the outward movement of TM6, and the distance between the two conserved tyrosine residues Tyr$^{5.58}$ and Tyr$^{7.53}$ represents an important microswitch in class A GPCR activation [70]. Residues from TM5 that interact with the ligand, such as 5.46, cause rearrangements in the NPxxY motif in the form of a twist, which reorients Tyr$^{7.53}$ towards Tyr$^{5.58,}$ forming a water-mediated interaction known as the Y-Y interaction [70,101]. Together with the displacement of TM6, captured by the distance between 3.50 and 6.34, the formation of the G protein binding site was established [70]. Therefore, we expected that the fully active conformation of the monomers would result in a short distance between the two tyrosines (Y-Y interaction). Conversely, we expected inactive conformers to exhibit longer distances between two tyrosine residues. Our observations for the monomers (Fig. S13) support these expectations. The **in-monomer** showed a short distance between TM3-TM6 and a large distance between Y and Y-Y. The **ar-monomer** had a larger distance between TM3-TM6 but a visibly shorter distance between Y-Y. For the **ac-monomer**, at some time points, the distances were even shifted towards an active conformation compared to those measured for the **ar-monomer**. When comparing the monomer and dimer configurations, it could be shown that some conformational changes occurred within the dimers (Fig. S14). While most of the protomers displayed properties similar to those of their uncomplexed monomers, the **ac-protomer** within the **ac-ar** configuration was found to be more active (fully activated) than the monomer only, compared to the partnered **ar-protomer.** However, the **ac-protomer** in the **ac-in** dimer was clearly shifted towards a more inactive conformation, displaying a short distance between TM3-TM6 and a larger distance between Y and Y-Y. We also monitored the comparison of the distances between the Cα atoms of residues 5.46–7.41 (TM5 bulge) and the ΔRMSD of two residues of the PIF motif (Ile$^{3.40}$ and Phe$^{6.44}$) (Fig. 3**, S15**). According to Fleetwood et al., the formation of a bulge on TM5 by residues 5.46 and 7.41 influences the intracellular distance between residues 3.40 and 6.44, which are part of the PIF (connector) motif [70]. These residues are also known to be in contact with highly conserved Asp$^{2.50}$ and NPxxY through a network of water molecules [70]. When analyzing the results for the free monomers (Fig. S15), it is clear that the **in-monomer** had the

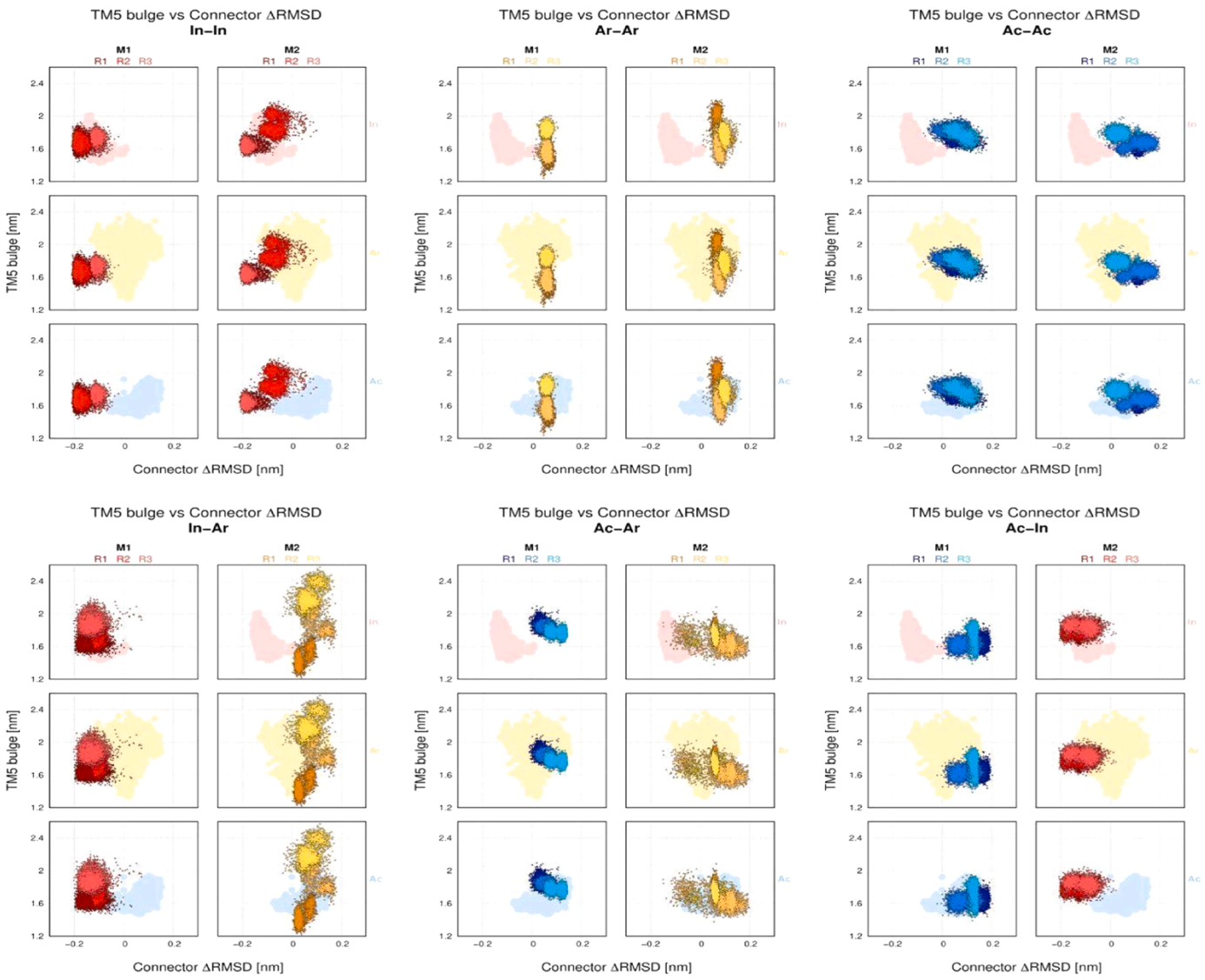

Fig. 3. Comparison of TM5 bulge movement and RMSD of residues I.340 and F.644 (connectors) for D_2R homodimer configurations. Comparison of Cα-distance between 5.46 and 7.41 and the RMSD of residues Ile3.40 and Phe6.44, which were measured for all protomers and replicates over time. For easier comparison, the distances of the individual monomers in the three activation states (in, ar, and ac) are shown as light-colored clouds in the background of three different lines. Conformations are color-coded as inactive red, arrestin yellow, and active blue.

distance of the TM5 bulge varied between 1.60 and 2.00 nm, while the ΔRMSD of the connector ranged between − 0.15 and − 0.10 nm. In contrast to the **in-monomer**, the ΔRMSD of the **ac-** and **ar-monomer** connectors was between 0.00 and 0.15 nm. In addition, the distance between the residues in the TM5 bulge showed a more dispersed distribution (range 1.40–2.20 nm) for the **ar-monomer** and was more concentrated (approximately 1.50–1.90 nm) for the **ac-monomer**. These findings were consistent with those reported by Fleetwood et al. (Fig. 4 of Fleetwood et al., panels d-f, [102]) and put the **ar-monomer** in an intermediate activation state compared with the fully activated **ac-monomer**. In the **in-in** dimer configuration (Fig. 3), there is a decrease in the ΔRMSD towards − 0.20 nm and a different behavior for the two protomers, with one accessing an intermediate conformation. In the **in-ar** and **in-ac** dimers, we also observed a high stability of the **in-protomer** in its inactive state. Both inactive and active conformations of the TM5 bulge were populated in the **ar-ar** dimer, reaching even higher values for the **ar-protomer** in the **in-ar** dimer. In contrast, the **ar-protomer** in the **ac-ar** dimer populates only active states. The **ac-protomer** is very stable in an active conformation in the **ac-ac**, **ac-ar**, and **ac-in** dimers.

Lu et al. tracked the angles between the centroids of the benzene rings of three phenylalanines (5.51, 6.44, and 6.45) over time. This analysis was replicated in the current study (Fig. S18) [103]. Upon activation, residues 6.44 and 6.45 moved towards residue 5.51, which then promoted an outward movement of TM6. Furthermore, all residues near the aromatic microdomain, where the rotamer toggle switch takes place, also move forward [86,103,104]. For the uncomplexed monomers, the **in-monomer** was constant at 50–60°, the **ar-monomer** was found at 70–90°, and the **ac-monomer** was found between 60° and 80°.

Upon closer examination of the properties of TM6, we observed that the conformational states of the individual monomers did not change significantly during simulation. However, the configurations of most dimers changed, with the exception of **in-conformers**. The **ac-protomer** in the **ac-in** configuration adopts the properties of an inactive conformer. In the **ac-ac**, **ar-ar**, and **ac-ar** configurations, one protomer appeared to be more active than the other, indicating that it may shift between a fully active conformation and an intermediate state that has several properties similar to the arrestin-bound conformation. This can also explain the differences between the protomers of the **ar-ar** configuration.

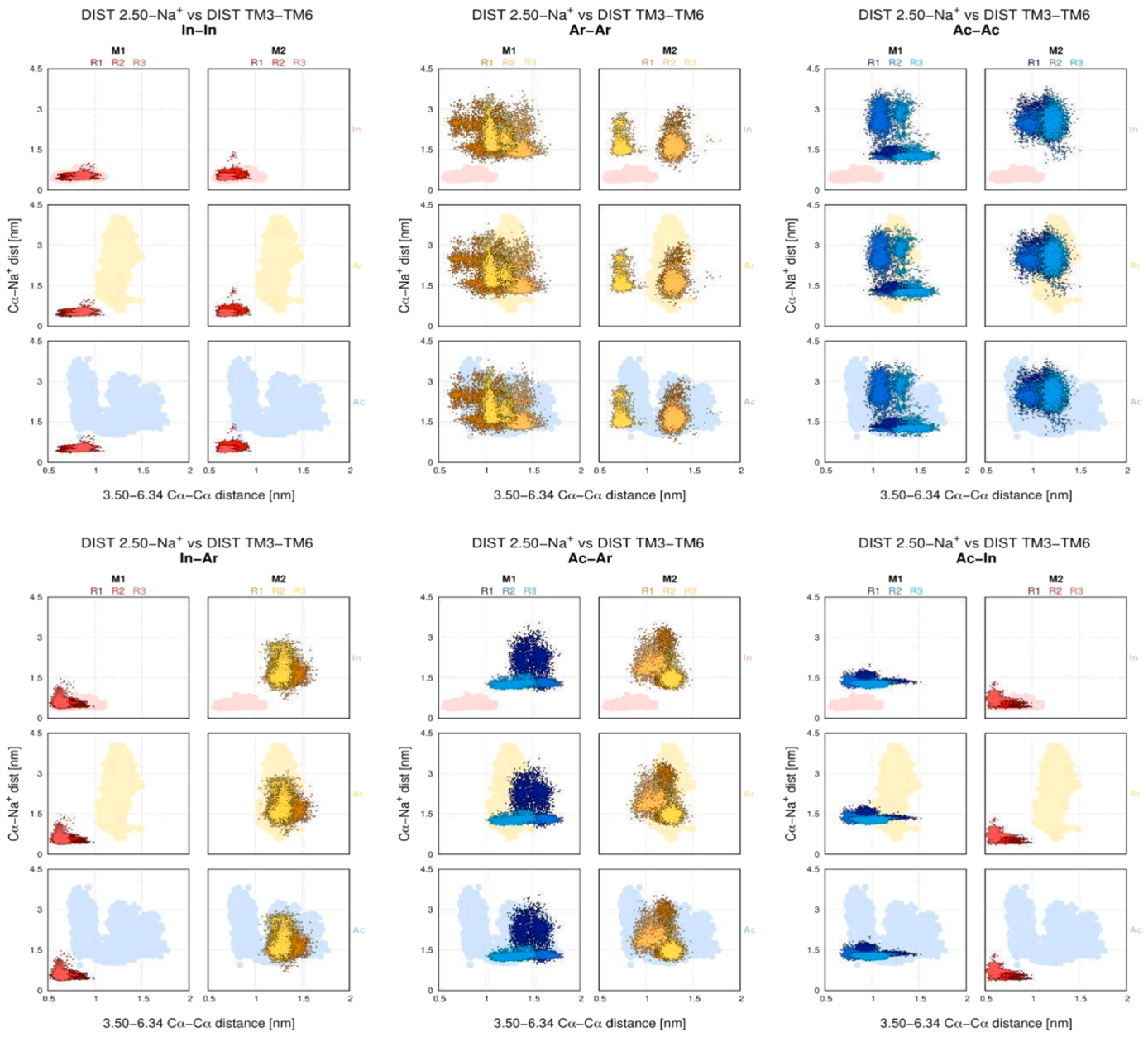

Fig. 4. Comparison of the disruption of the ionic lock represented as a distance between 3.50 and 6.34, and the distance between $Asp^{2.50}$ and its closest sodium for the D_2R homodimer configurations. Comparison of the Cα-distance between 3.50 and 6.34 and the distance between the Cα atom of the conserved residue $Asp^{2.50}$ and sodium (Na+), which were measured for all protomers and replicates over time. For easier comparison, the distances of the individual monomers in the three activation states (in, ar, and ac) are shown as light-colored clouds in the background in three different lines. Conformations are color-coded as inactive red, arrestin yellow, and active blue.

3.7.2. The collapse of the sodium pocket

Numerous studies have shown that ligand binding and activation of class A GPCRs leads to changes around the CWxP, TM5, and PIF motifs, resulting in the collapse of the sodium pocket around the conserved aspartic acid 2.50. This process involves dehydration, displacement of the sodium ion, and protonation of $Asp^{2.50}$, ultimately leading to rewiring of the NPxxY motif [69–73]. The allosteric Na^+ ion forms strong interactions with residues $Asp^{2.50}$ and $Ser^{3.39}$ and several water molecules, all stabilizing the inactive state of GPCRs [70,105–107]. Upon activation, the ionic lock is disrupted, and the sodium pocket around $Asp^{2.50}$ collapses, releasing sodium into the intracellular space [71].

In our study, we also monitored changes in these two regions by calculating the distance between the Cα atom of $Asp^{2.50}$ and the closest sodium atom, and compared this to the distance between the Cα atoms of residues $Arg^{3.50}$ and $Thr^{6.34}$, the ionic lock (Fig. 4, **S19**). When looking at the individual monomers, the **in-monomer** appeared to have a short distance towards sodium, whereas in the **ac-** and **ar-monomers,** sodium was located more than 1.5 nm away from $Asp^{2.50}$ (Fig. S19). The distance between $Arg^{3.50}$ and $Thr^{6.34}$ was less than 1.0 nm for the **in-monomer**, indicating that the ionic lock had not yet been disrupted. Distances above 1.0 nm were considered indicators of activated conformations, which was the case for **ac-** and **ar-monomers** (1.0–1.5 nm). When comparing these results with the dimer configurations (Fig. 4), we see that all **in-protomer**, **ac-ac**, **ar-ar**, and **in-ar** configurations have metrics similar to their individual uncomplexed forms. In the **ac-ar** configuration, the ionic lock residues of the **ac-protomer** were more widely separated than those of the uncomplexed monomers, and the

same was true for **ar-protomer.** In the **ac-in** dimer, the **ac-protomer** had properties of an inactive receptor, with approximately 1.5 nm and a closed ionic lock (0.5–1.5 nm). Another indicator of disruption of the sodium pocket is the number of water molecules in its vicinity. Therefore, we calculated the number of water molecules within a 0.8 nm radius surrounding $Asp^{2.50}$ (Fig. 5). The number of water molecules was consistently higher (~30) in the **in-conformer** than that in the **ac-** and **ar-conformers** (~10).

Interestingly, a clear distribution between the conformers was observed for the individual monomers. A comparison of these findings with those of the dimer configurations showed that the number of water molecules in the **in-in** configuration was similar to that of individual monomers. Interestingly, the average number of water molecules differed between the two protomers within the **ac-ac** dimers. In this configuration, protomer 2 contained approximately twice as many water molecules as protomer 1 did. Furthermore, the number of water molecules in the **ar-ar configuration** is significantly reduced by 50% upon dimerization. For the **in-conformation,** we found that it remained inactive regardless of the partnered monomer, whereas the **ac-** and **ar-conformations** behaved similarly to the active conformers (see Fig. 5).

3.7.3. *Hydrophobic lock*

After GPCR activation, breaking of the hydrophobic lock comprising the hydrophobic residues at positions $3.43Leu^{3.43}$, $Val^{6.40}$, and $Leu^{6.41}$ is another important microswitch event that loosens the connection between TM3 and TM6 [87,103]. It also promotes the breaking of the ionic lock between $Arg^{3.50}$ and $Glu^{6.30}$, which finally releases TM6 outwards [87,103,108]. To observe the status of the hydrophobic lock, we measured the area of the angle composed of the Cγ atom of $Lys^{3.43}$, Cβ atom of $Val^{6.41}$, and Cβ atom of $Ile^{6.40}$ over time, as described by Lu et al. (Fig. S20) [103]. The authors suggested that an area of approximately 15 $Å^2$ represents an inactive state, 10–20 $Å^2$ indicated an intermediate state, and everything above 20 $Å^2$ represents the active state of the GPCR [103]. We only found breaking of the hydrophobic lock upon activation in the **ac-conformers**, while all **in-protomers** behaved like inactive conformers, regardless of their partners.

3.7.4. *Microswitch: Transition of dihedral angles χ_1 and χ_2 tyrosine 7.53*

Upon class A GPCR activation, the highly conserved $Tyr^{7.53}$ undergoes conformational transitions between its dihedral angles χ_1 and χ_2, according to Yuan et al. [100]. Following the angles over time (Figs. S21 and S22), we observed major differences between the different conformational states of the individual monomers and the dimer configurations. The χ_2 angle displayed several large conformational shifts, primarily for **ac-** and **ar-conformers** at any combination undergoing large movements, whereas **in-conformers** were more restricted. When comparing the dihedral angles χ_1 and χ_2 (Figs. S23 and S24), it became clear that some of the configurations showed more variation than the others. The smaller variation in χ_1 can be explained by the large rotations at this angle, which lead to steric clashes with the protein backbone. We also observed a lower rotation in $Tyr^{7.53}$ for **in-conformers**, while rotations of χ_2 in **ar-** and **ac-conformers** indicated that these conformations switch from active to inactive conformations. Moreover, the **ac-protomers** in the mixed configurations showed less variation than those in the monomer form, which can be explained by the less space available for conformational transitions into a fully active conformation when involved in a complex.

3.7.5. *Transitions in the NPxxY motif*

According to Leioatts et al. [96] and Dror et al. [109], the deactivation of class A GPCRs consists of a two-step process, in which the NPxxY motif first undergoes transitions towards an inactive conformation, followed by ionic lock closing as TM6 moves inward to the helical bundle. Hence, the RMSD of NPxxY and the distance between the Cα-atoms of residues of the ionic lock $Arg^{3.50}$ and $Glu^{6.30}$ should enable mapping of this process [96]. When we calculated these structural properties for different D_2R homodimer configurations, we observed that specific values could be determined for individual monomers based on their conformation (Fig. 6**, S25**).

For the **in-monomer**, the distributions of both the RMSD of NPxxY

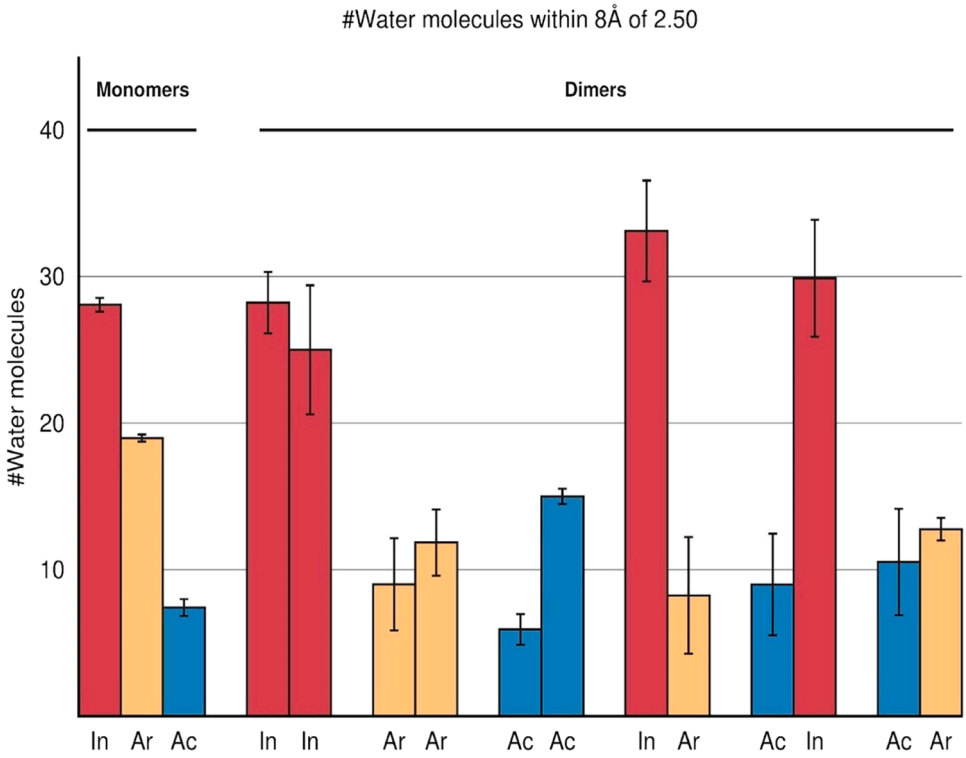

Fig. 5. The number of water molecules within 8 Å of Asp2.50 for the D2R homodimer configurations. The number of water molecules within 8 Å of the conserved residue Asp2.50 for the complete simulation time are represented as mean ± SEM. Conformations are color-coded as inactive red, arrestin yellow, and active blue.

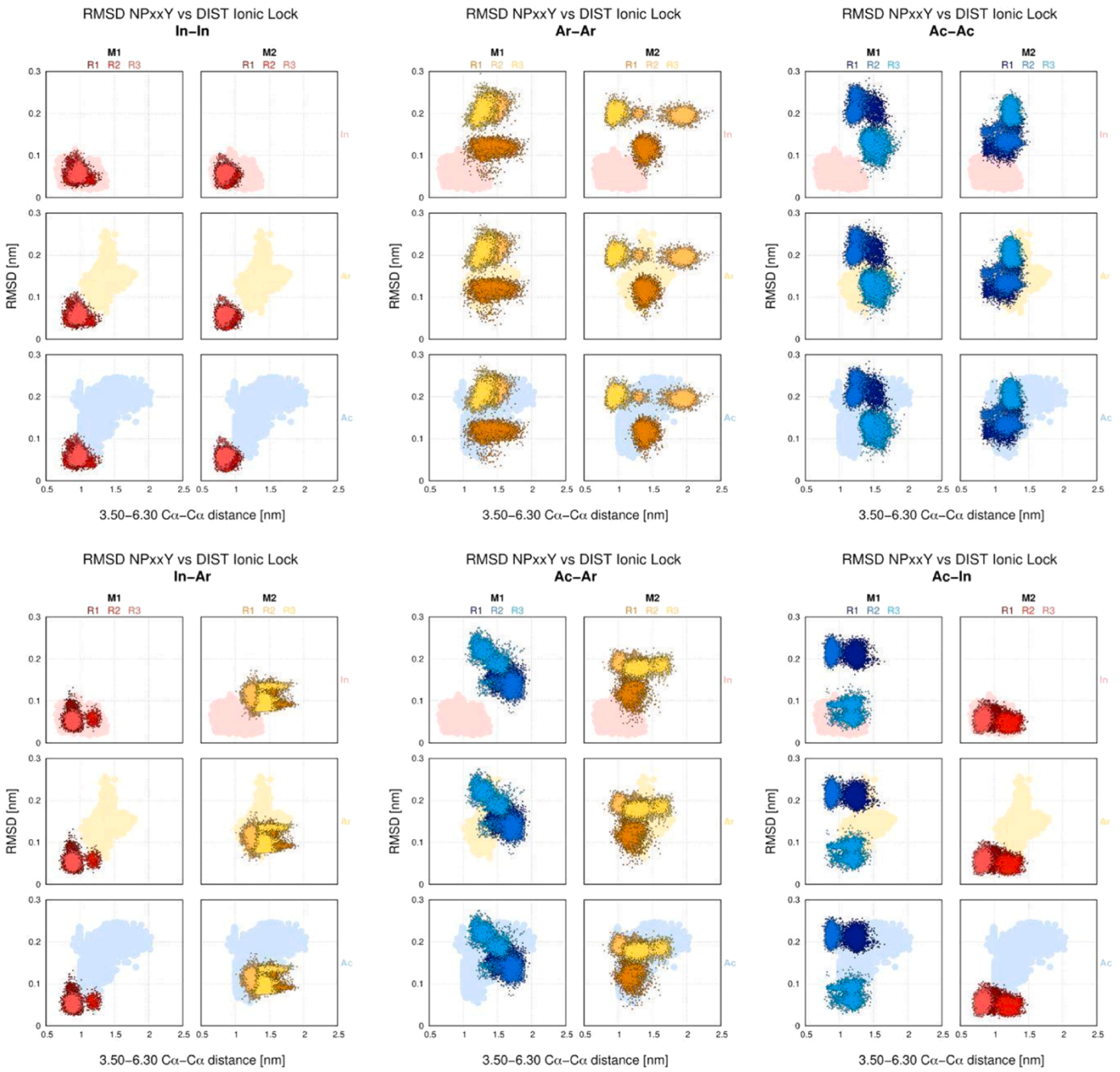

Fig. 6. Comparison of the RMSD of NPxxY and the distance between Cα-atoms of residues of ionic lock 3.50 and 6.30. Comparison of the RMSD of NPxxY and the distance between Cα-atoms of residues of ionic lock 3.50 and 6.30, for which RMSD and distances [nm] of the uncomplexed monomers are shown as light-colored clouds in the background. Conformations are color-coded as inactive red, arrestin yellow, and active blue.

and the distance of the ionic lock were relatively small and concentrated, indicating that the ionic lock was closed in the inactive conformation and no significant transitions occurred in the NPxxY motif. (Fig. S25). For the **ar-monomer,** the RMSD of NPxxY varied more than the ionic-lock distance. For the **ac-monomer**, the RMSD of the NPxxY motif was more diverse, and the distance of the ionic lock increased. In the dimer configurations, the protomers remained inactive in inactive conformations, whereas differences between monomers and complexes were observed for the **ac-** and **ar-conformers** (Fig. 6). It is worth noting that the **ar-protomers** adopted inactive-like conformations in the **in-ar** dimer, and the **ac-protomers** were distributed over both active and inactive-like populations in the **ac-in** dimer.

We analyzed the changes in the NPxxY motif by comparing ΔSASA with the RMSD of this motif (Figs. S26 and S27). When examining the individual monomers, we found that for the **in-monomer**, the RMSD was between 0.0 and 0.1 nm, and the ΔSASA was between 9% and 18%, while the RMSD was increased to 0.1–0.2 nm for the **ar-monomer** and the ΔSASA did not change significantly. For the **ac-monomer**, the RMSD increased above 0.2 nm, and the ΔSASA was spread between 9% and 20%. In the dimer configurations, the **in-conformers** always displayed the same values regardless of the partner, whereas more variation was observed for the other conformers (Fig. S27). Analysis of the NPxxY motif in the monomer and dimer configurations confirmed the results obtained for other motifs. The **in-conformer** is always inactive, whereas the **ar-ar**, **ac-ac**, and **ac-ar** configurations display properties similar to those of the activated receptors.

3.7.6. Sizes of G protein- and β-arrestin-binding areas

The sizes of the binding sites for G protein and β-arrestin were determined using the SASA values of relevant residues, which were then normalized to the $SASA_{max}$ values determined earlier for each type of amino acid. The sizes (expressed as a percentage) were calculated over time (**Figures 28** and **S29**), and then averaged and compared within the different dimer configurations (Fig. 7). According to Yuan et al., small binding areas suggest an inactive state of the receptor, as there is no space available for binding a G protein or β-arrestin [100]. We observed the smallest areas of binding sites for the inactive protomers (Fig. 7). The largest values were determined for the **ar-ar** and **ac-ac** dimer configurations. Additionally, the ratios between the protomers were consistent for both G protein- and β-arrestin-binding sites.

4. Discussion

4.1. Dimer configurations are stable

The goal of our study was to design a straightforward protocol for building GPCR homodimers, identifying their most stable interfaces, and complementing previous studies on other GPCR dimers, including those of Kaczor et. al [27,92,93]. We used the D_2R homodimer as a case study because experimental data are available for this system.

Our results show that different dimer configurations can form stable TM4-TM5-TM4-TM5 interfaces regardless of whether the partnered protomers are active or inactive. This is in line with experimental studies showing that the dimers seem to be pre-assembled independently of ligands and therefore also independent of the conformation of partnered protomers. However, we found that the inactive conformation was

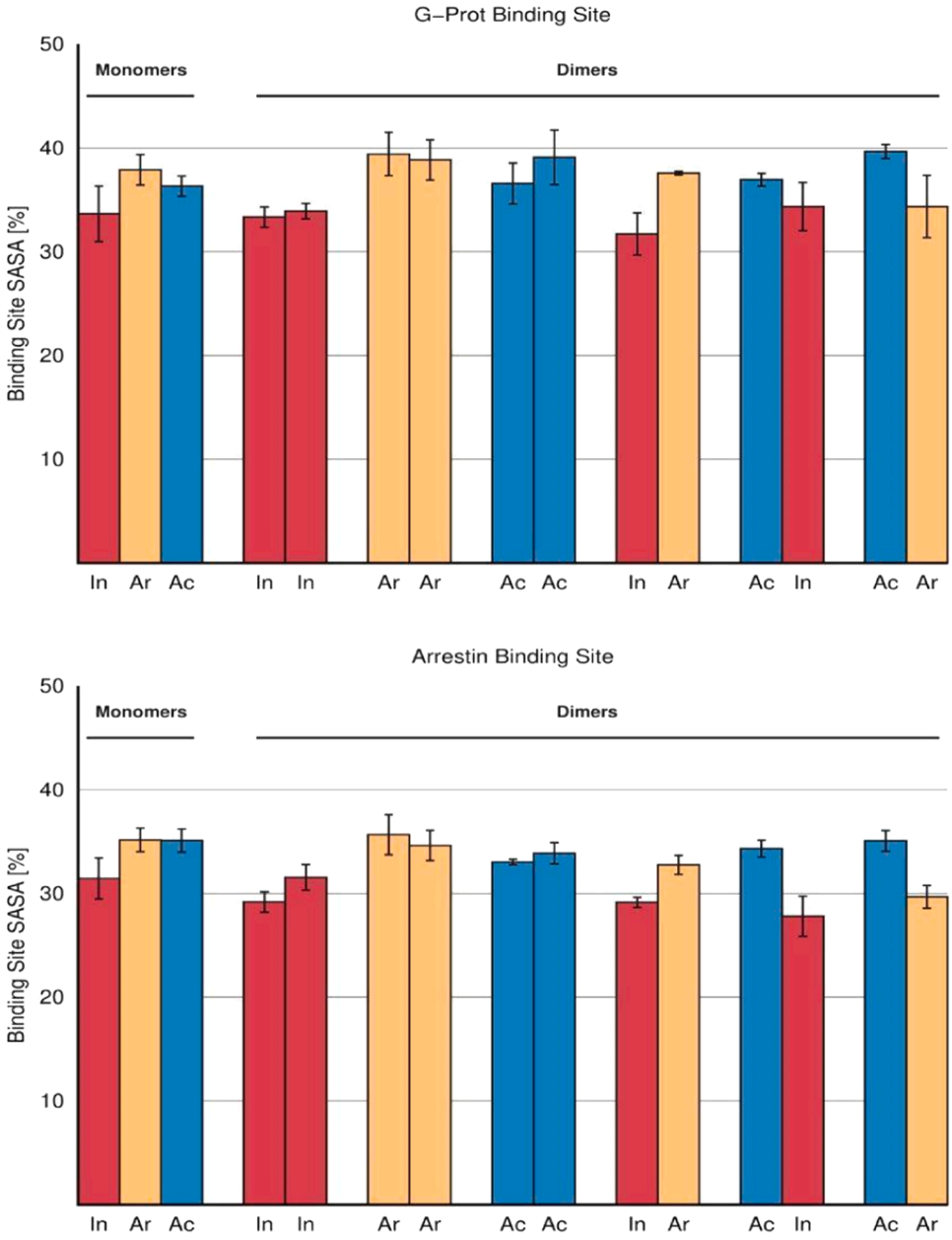

Fig. 7. Size of the binding sites for G-protein and β-arrestin. The sizes of the G protein and β-arrestin binding sites [%] were determined using the SASA values of binding site residues. These values were then normalized to the SASAmax values determined for each type of amino acid. The volumes are shown as the mean ± SEM. Conformations are color-coded as inactive red, arrestin yellow, and active blue.
Retrieved from Preto et al. (2020) [52].

maintained in all combinations, whereas the **ac-** and **ar**-conformations were either active or desensitized (activated state). We observed variations in some metrics for **the ac-** and **ar**-conformers, particularly in terms of helix movement. The **ac-ac** combination was found to be active, whereas the individual monomers were found in an intermediate conformation between inactive and active. This indicates that the active protomers stabilize each other's active conformations. Most notably, we observed that an active protomer adopts properties of an inactive conformation when paired with an inactive protomer, particularly in terms of helix movement, transitions in the NPxxY motif, and the position of the ionic lock. The latter was only observed for the **in-ac** dimer. Additionally, we found that this ionic lock was broken for **the ac conformers** in all combinations, even when paired with an inactive protomer. The addition of G proteins may alter this behavior. We verified that the dimers with the TM4-TM5-TM4-TM5 proposed interface followed the same behavior as previously described for a similar configuration in the serotonin$_{1A}$ receptor [110,111].

The **in-conformer** was always inactive, whereas the **ar-ar**, **ac-ac**, and **ac-ar** configurations displayed properties similar to those of activated receptors. Analyses of macro- and microswitches revealed that the inactive configuration was unperturbed by its partnered protomer, whereas in the **ac-in** dimer, the active protomer adopted the properties of an inactive receptor. In some cases, the arrestin configuration displayed properties of an active receptor in the absence of an agonist, suggesting that a switch to another meta-state within the dimerization process was observed. In summary, the relevant residues found in our study were in agreement with the experimental data, thus validating our computational protocol. This method can be easily adapted to heterodimers and may also be extended by adding additional proteins, such as G proteins or β-arrestins.

4.2. The central role of transmembrane domains 4 and 5 in dimer formation

TM1, TM4, and TM5 bear the largest membrane-accessible areas, indicating their importance in the establishment of protein-protein interactions [14]. Several studies have revealed the importance of TM4 and TM5 in homo- and heterodimer formation [19,44,110,112–119]. However, many other interface points have also been identified, including TM5-TM6-TM5-TM6 [23,120], TM1, TM2, HX8, and ECL1 [13,27,115,119,121,122]. Here, we observed that the involvement of TMs changed depending on the combination of conformers. A symmetric TM4-TM5-TM4-TM5 interface was determined for most configurations, except for two very different arrangements: **ac-in** (TM1-TM2-TM4-TM5) and **in-ar** (TM3-TM4-TM4-TM5). This is consistent with the "rolling dimer" interface model proposed by Dijkman et al., which suggests that GPCRs can exploit multiple interaction interfaces that can coexist and interconvert [123]. In the **ac-in** and **in-ar** dimers, the interaction between GPCRs led to the establishment of asymmetrical and larger interfaces in comparison to the **ac-ac** configurations, and were therefore closer in size to the **in-in** dimer.

Overall, our findings are in agreement with earlier experimental studies by Guo et al., who reported that TM4-TM5 is the most likely physiological interface of the D_2R homodimer [16,17,44]. However, other studies have supported these alternative possibilities. Marsago et al. showed that the D_3R homodimer has two potential interfaces: one involving residues from TM1, TM2, and HX8 and the other involving TM4 and TM5 [5,48]. TM3 has also been found at the A2AR-D2R heterodimer interface [43]. TM6 is unlikely to play a significant role in complex formation, as it would likely cause steric clashes between the protomers upon activation due to its outward movement [123–125].

4.3. Transmembrane domain and loop involvement in dimer formation

The interfacial characterization of all configurations in this study highlights the important role of TM regions and loops in driving complex formation. This finding is in agreement with those reported by Simpson et al. [45], Pulido et al. [126], and Filizola et al. [116] pinpointing ICL2 and ECL2 as particularly relevant, which has also been observed in other studies [127]. ICL3 also forms relevant interactions, particularly with the C-terminal region. However, it is difficult to fully assess their involvement because these loops are very large and flexible and cannot be well captured by experimental techniques or modeled by computational methods. Consequently, analysis of the ensemble of conformations involving these loops remains elusive. We identified a subset of highly conserved residues that were relevant for all dimer configurations determined in the static structure (PRODIGY), considering the dynamic behavior of the dimers (SASA) during the simulation:160ALA (ECL2), $Arg^{4.40}$, $Val^{4.44}$, $Ile^{4.48}$, $Val^{4.51}$, $Leu^{4.52}$, $Thr^{4.55}$, $Pro^{4.59}$, $Tyr^{5.41}$, $Val^{5.45}$, $Val^{5.49}$, and $Val^{5.53}$. Comparing these findings with those of Guo et al. [16–18], some differences and similarities were observed. For example, $Arg^{4.40}$, $Val^{4.44}$, $Ile^{4.48}$, $Val^{4.51}$, $Thr^{4.55}$, and $Pro^{4.59}$ residues were involved in both studies. Guo and coworkers [16–18] stated that residues $Trp^{4.50}$, $Phe^{4.54}$, $Cys^{4.58}$, and $Arg^{4.43}$ were relevant to mediate the crosstalk between the protomers in an active conformation. Herein, we observed their participation only in **ac-** and **ar-conformers**. Guo et al. reported different amino acid combinations for TM4-TM5 (inactive dimer configuration) and TM4-TM4 (active dimer configuration) [17]. It has also been reported that the replacement of $Cys^{4.58}$ leads to the elimination of receptor crosstalk, and that this amino acid is relevant for the active TM4-TM4 conformation of the D_2R homodimer. In our study, $Cys^{4.58}$ was present in both protomers of the **ac-ac** configuration with the TM4-TM5-TM4-TM5 interface and in both protomers of the **ac-ar** dimer (Table S2). Guo et al. also identified other residues relevant to an additional interface involving TM1 ($Pro^{1.30}$, $Tyr^{1.34}$, $Tyr^{1.35}$, $Leu^{1.38}$, $Leu^{1.41}$, $Asn^{1.50}$, $Arg^{1.59}$, and $Phe^{7.65}$) [18]. Residues $Tyr^{1.34}$, $Tyr^{1.35}$, and $Arg^{1.59}$ were also relevant for our dimer configurations. Residue $Arg^{1.59}$ could be identified on the **ac-protomer** of **ac-in** and on the **ar-protomer** of **in-ar** [18]. Lastly, Wouters et al. suggested the formation of a TM5-TM6-TM5-TM6 interface and that $Tyr^{5.48}$ and $Phe^{6.52}$ are important for dimerization [23]. While $Phe^{6.52}$ was not found at any D_2R homodimer, $Tyr^{5.48}$ was found twice on the **in-in** dimer, once on the **ac-ac**, once on the **ar-ar**, on the **in-protomer** of the **ac-in,** and in the **in-ar** configuration.

The highly prevalent residues identified in our study (mostly from TM4 and TM5) were nonpolar and therefore complementary to establishing stable interfaces. These types of residues are expected, considering the nature of TMs, because exposing charged or polar residues to the lipid bilayer could lead to transient dimerization [44,128]. It has previously been shown that at least two adjacent arginine, glutamic acid, aspartic acid, or phosphorylated amino acid residues are sufficient to induce stable non-covalent complexes in heterodimers [117,129,130]. From our set of highly preserved residues, $Arg^{4.40}$, $Thr^{4.55}$, and $Tyr^{5.41}$ were the most capable of establishing electrostatic interactions.

Our results indicated the involvement of ICL2, ECL2, ECL3, and TM3 in stabilizing interactions. This is also in line with a study on opioid receptor homodimers, which showed that residues from loops TM3 and TM2 stabilize the TM4/TM5 interface [131]. In the same study, the authors described a specific subset of conserved residues (4.39, 4.43, 4.47, 4.50, 4.51, 4.54, and 4.62), similar to our identified prevalent residues in the dopamine receptor [131]. In another study investigating the D_1R-D_2R heterodimer, mutations in valine, proline, and serine residues were found to alter the dimerization propensity of D_1R and D_2R [132]. The authors also stated that valine and proline residues promoted the formation of the D_2R homodimer interface [132]. Interestingly, Johnston et al. also identified two important valine residues, whereas we found five across all configurations [131].

H-bonds were predominant and involved several residues from the TMs and loops, particularly in the **in-in**, **ac-ac**, **ac-in**, and **in-ar** dimer configurations. In contrast to these types of interfaces, most interactions were found between TMs for the **ar-ar** configuration, especially involving TM5. In a comprehensive study involving the $A_{2A}R$-D_2R

heterodimer, it was also shown that TM5 was responsible for the interactions between the two protomers, thus promoting the negative allosteric effect of the adenosine receptor on dopaminergic signaling [43,133]. However, most interactions, such as π-cation, π-stacking, T-stacking, or even salt bridges, are formed between loops or between a loop and TM. Hence, loops can be the main drivers of interface formation and provide extra affinity to stabilize the final dimers. Similarly, O'Dowd et al. found a pair of adjacent glutamic acids (at the C-terminus of D_1R) and a pair of adjacent arginines (from ICL3 of D_2R) in the D_1R-D_2R heterodimer interface, forming stable electrostatic interactions [134,135].

4.4. The conformational status of individual protomers affects the macro- and microswitches

Macro- and microswitches of class A GPCRs are involved in conformational rearrangements upon ligand binding to promote the outward movement of TM6 and its activation by enabling the necessary space for the binding of a G protein (Fig. S8) [87,135]. Our results indicated that the conformational status of the protomers remained consistent over time and that the movements of the relevant TMs (TM3, TM5, TM6, and TM7) were in agreement with what is known about the mechanism of class A GPCR activation.

However, two motifs remained active for **ac-conformers** in all combinations: (i) the distance between the TM5 bulge and the ΔRMSD of the connector motif and (ii) the sodium-binding pockets. This can be attributed to the large volume occupied by the bound bromocriptine ligand in the orthosteric binding pocket, which leads to partial activation of some motifs, such as CWxP and the sodium-binding pocket. These rearrangements did not extend throughout the receptor to the ionic lock, NPxxY, or other motifs because of the presence of the protomer in an inactive conformation. This would be seen as negative allosteric crosstalk, which has been reported for many heterodimers involving DRs [4]. In contrast, the **ar-conformer** within the **ac-ar** dimer appeared to possess a collapsed sodium pocket, although no ligand bound to this conformer.

In contrast, the **ar-protomer** within the **in-ar** configuration displayed the same properties as its individual monomer, namely, the properties of an active receptor, which seemed not to be influenced by its inactive protomer. **Ac-ac, ar-ar** and **ac-ar** dimers displayed larger variations after simulation, remaining, however, in an active form. Interestingly, we found that one protomer in the ar-ar configuration displayed asymmetric properties of active receptors. The outward movement of TM6 was not as pronounced as that of the **ar-conformers**. In fact, one protomer of the **ar-ar** dimer transitioned to an active conformation when comparing the distance of the ionic lock and Y-Y motif, and showed that the **ar-protomers** in the **ar-ar** dimer behaved differently, pointing to two distinctive active-like states. We also observed slight differences between the homo-conformation and mixed conformation. The **ac-ac** configuration displayed properties of activated protomers, but it was difficult to assign the conformational status of the **ac-ar** dimer. For some structural properties, the **ar-protomer** adopted an active conformation, whereas the **ac-protomer** appeared to be less active in the **ac-ar** configuration.

According to Caniceiro et al., most studies reported positive crosstalk for DR-DR dimers, and in some cases, this resulted in a hyperdopaminergic response, which other authors have linked to schizophrenia or the use of amphetamines [4134,136]. Such an effect would be represented by the configurations **ac-ac**, **ar-ar,** and **ac-ar**, where at least one bromocriptine was bound to the dimer. This is also in line with the results of Guo et al., who stated that ligand binding to one of the protomers would be enough to bind a G protein and cause conformational arrangements within the ligand-free protomer towards an active-like state [18,137,138]. For instance, a study of D_1R-D_3R heterodimers showed that coactivation of both receptors leads to a negative interaction at the level of adenylate cyclase, recruitment of β-arrestin-1, and selective activation of MAPK signaling mediated by a G protein-independent mechanism [133,139,140]. Likewise, it has been reported that the D_2R-D_3R heterodimer can suppress forskolin-induced activation of adenylate cyclase at very high levels without the need for ligands [35,141,142]. One possible explanation for this is that in the **ac-in** configuration, the **ac-protomer** adopts the conformation of an inactive receptor. The asymmetrical TM4-TM5-TM4-TM5 interface was not found for this dimer, which may prevent both protomers from reaching active-like conformations, as the **ac-protomer** does not contribute to TM4 at the interface.

This also supports the idea that in the **in-ar** configuration, where the **in-protomer** contributes TM3 and TM4 to the interface and the **ar-conformer** contributes TM4 and TM5, the correct conformations can be achieved, and both protomers are in an inactive or activated/intermediate state due to the absence of a ligand. Additionally, the results for the hydrophobic lock showed that the **ac-ar** configuration had the highest active-like values for both protomers, suggesting that one **ac-monomer** alone may not be fully activated in the absence of a G protein. As only one protomer in the mixed conformation had a smaller binding site for the G protein, it could be assumed that it would be possible to bind only one G protein. Nevertheless, because **ac-ac** and **ar-ar** dimers have similar binding site sizes for both protomers, this hypothesis does not seem to hold. In fact, the composition of the dimer interface and the presence of an agonist may affect the size of the G protein binding area (and β-arrestin), supporting the 'rolling dimer' interface model proposed by Dijkman et al.[123].

4.5. Key residues and pathogenic relevance

According to a study by Caniceiro et al., mutations in certain residues can have pathological consequences in DRs [143]. For example, $Arg^{1.59}$, $Thr^{3.52}$, $Arg^{4.40}$, $Arg^{4.41}$, and $Val^{5.49}$ have been found in different dimer configurations. Guo et al. [18] as well as other authors [110,144] reported that $Arg^{4.40}$, $Arg^{4.41}$, and $Arg^{1.59}$ were key residues, which led to changes in the secondary structure of the helix when mutated [145]. In addition, $Arg^{4.40}$ was identified as a key residue in another study involving the 5-hydroxytryptamine 1A receptor and orexin receptor 1 heterodimer, changed its interface from TM4-TM5 in the basal state to TM6 in the active conformation [144]. Zhang and coworkers also showed that mutations of $Arg^{4.40}$ can affect G protein binding [144]. The ability of arginine residues to better accommodate hydrophobic mismatches at TM4 of GPCRs may explain why the $Arg^{4.40}$ can affect G protein binding [146,147]. Residues at positions 3.52 and $Arg^{4.41}$ have been found to be important for the formation of the TM4-TM5 interface for serotonin receptors [110]. $Arg^{4.40}$ and $Arg^{4.41}$ interacted with the corresponding amino acids in the opposite protomer. $Arg^{1.59}$ has been reported to be relevant for G protein binding, particularly in the interaction between $G\alpha_s$ and $G\alpha_{i1}$ for the β_1-adrenoceptor [148]. According to Wang et al., residues at position 3.52, $Thr^{3.52}$ for D_2R, would only be relevant for G protein binding if they were hydrophobic [149,150]. Overall, residues on TM4, such as $Arg^{4.40}$ and $Arg^{4.41,}$ are important for homo- and heterodimers comprising the TM4-TM5 interface and can be pathogenic when mutated. In addition, mutations in residues at positions 1.59 and 3.52 may affect G protein binding.

Understanding GPCR homo- and heterodimers is of key importance for the development of new biased drugs [151] because these dimers can display unique allosteric properties and the interface can be targeted with agents that either stabilize or disrupt the dimerization process.

5. Conclusion

The goal of our study was to develop a workflow for identifying GPCR homo- and heterodimer interfaces and to validate them using available experimental data. As a proof of concept, we chose the D_2R-homodimer as it is a well-studied GPCR. We found that the D_2R protomer interaction types were very specific to the dimer configuration and

the formed interfaces and that they were stable over time, suggesting a conserved pattern. Most interactions were formed by loops (especially ICL2 and ECL2) rather than TMs because loops have a higher electrostatic character, whereas TMs are mostly composed of nonpolar amino acids at favorable positions in the lipid bilayer. Highly conserved residues in TM4 and TM5 were rarely involved in forming interactions, and a large interface area was correlated with the establishment of stabilizing interactions by TM residues. Our models were in good agreement with those reported in the literature, including the identification of the roles of important residues and TMs. For example, TM4 and TM5 were found to be critical for dimer formation, regardless of the conformational status of the protomers, which is consistent with experimental findings. In addition, considering the conformational states of the protomers together with all geometrically possible interfaces, we are able to cover all the possibilities in which GPCR dimers can exist and can ultimately mimic states where crosstalk within dimers takes place.

Using different conformations of one receptor, we gained insights into the dynamic nature of the D_2R homodimer by mapping and comparing the known macro- and microswitches of class A GPCR activation. We found that the proposed dimer interfaces are physiologically stable, and that different homodimer configurations and interfaces are possible, which are highly dynamic and possess fully or partially adapting features of activation/inactivation. Key conformational changes relevant to dimer function and signaling were also observed. We also identified a subset of mostly nonpolar key residues present in all dimer configurations located on TM4 and TM5 and observed that loops and neighboring TMs significantly contribute to dimer formation. It should also be noted that large conformational transitions in GPCRs require large-scale MD simulations, as such processes usually occur on a μs timescale [152–154].

This protocol can be easily applied to identify the interface of any type of GPCR homo- or heterodimer and will be a useful tool for understanding the molecular and structural properties of other dimers. Furthermore, it can be extended by adding ligands, G proteins, and β-arrestins and will be useful for the development of dimer-targeting pharmaceuticals that target different pathological conditions.

Funding

This work was supported by the European Regional Development Fund through the COMPETE 2020–Operational Programme for Competitiveness and Internationalization and Portuguese National Funds via Fundação para a Ciência e a Tecnologia (FCT) [LA/P/0058/2020, PTDC/QUI-OUT/32243/2017, DSAIPA/DS/0118/2020, UIDB/04046/2020, UIDP/04046/2020, UIDB/04539/2020, UIDP/04539/2020 and CEECIND/02300/2017]. This work was produced with the support of the Laboratory for Advanced Computing at the University of Coimbra, and it was funded by FCT I.P. under the Advanced Computing Project CPCA/A2/7219/2020. B.B. and C.A.V.B. were supported by the FCT through PhD scholarships SFRH/BD/149709/2019 and SFRH/BD/145457/2019.

CRediT authorship contribution statement

Beatriz Bueschbell: Methodology, Data curation, Visualization, Software, Validation, Formal analysis, Writing – original draft, Writing – review & editing. **Pedro R. Magalhães:** Methodology, Data curation, Visualization, Software. **Carlos A.V. Barreto:** Software. **Anke C. Schiedele:** Writing – review & editing, Funding acquisition, Supervision. **Miguel Machuqueiro:** Writing – review & editing, Funding acquisition, Supervision. **Irina S. Moreira:** Writing – review & editing, Funding acquisition, Supervision, Conceptualization, Resources, Project administration. **Rita Melo:** Funding acquisition. All authors have commented on and approved the manuscript.

Declaration of Competing Interest

None.

Acknowledgments

We thank Agnieszka A. Kaczor for sharing the tcl script and Tiago Barbosa for his help with scripting parts of the analysis workflow.

Appendix A. Supporting information

Supplementary data associated with this article can be found in the online version at doi:10.1016/j.csbj.2023.08.032.

References

[1] Sriram K, Insel PA. G protein-coupled receptors as targets for approved drugs: how many targets and how many drugs? Mol Pharm 2018;93:251–8.
[2] Rosenbaum DM, Rasmussen SGF, Kobilka BK. The structure and function of G-protein-coupled receptors. Nature 2009;459:356–63.
[3] Fredriksson R, Lagerström MC, Lundin L-G, Schiöth HB. The G-protein-coupled receptors in the human genome form five main families. Phylogenetic analysis, paralogon groups, and fingerprints. Mol Pharm 2003;63:1256–72.
[4] Caniceiro AB, Bueschbell B, Schiedel AC, Moreira IS. Class A and C GPCR dimers in neurodegenerative diseases. Curr Neuropharmacol 2022. https://doi.org/10.2174/1570159×20666220327221830.
[5] Hiller C, Kühhorn J, Gmeiner P. Class A G-protein-coupled receptor (GPCR) dimers and bivalent ligands. J Med Chem 2013;56:6542–59.
[6] Somvanshi RK, Kumar U. Pathophysiology of GPCR homo- and heterodimerization: special emphasis on somatostatin receptors. Pharmaceuticals 2012;5:417–46.
[7] Guo H, An S, Ward R, Yang Y, Liu Y, Guo X-X, et al. Methods used to study the oligomeric structure of G-protein-coupled receptors. Biosci Rep 2017:37. https://doi.org/10.1042/BSR20160547.
[8] Schiedel AC, Kose M, Barreto C, Bueschbell B, Morra G, Sensoy O, et al. Prediction and targeting of interaction interfaces in g-protein coupled receptor oligomers. Curr Top Med Chem 2018;18:714–46.
[9] Fuxe K, Borroto-Escuela DO, Marcellino D, Romero-Fernandez W, Frankowska M, Guidolin D, et al. GPCR heteromers and their allosteric receptor-receptor interactions. Curr Med Chem 2012;19:356–63.
[10] Quitterer U, AbdAlla S. Discovery of pathologic GPCR aggregation. Front Med 2019;6:9.
[11] Sarasola LI, Del Torrent CL, Pérez-Arévalo A, Argerich J, Casajuana-Martín N, Chevigné A, et al. The ADORA1 mutation linked to early-onset Parkinson's disease alters adenosine A1-A2A receptor heteromer formation and function. Biomed Pharm 2022;156:113896.
[12] Shonberg J, Scammells PJ, Capuano B. Design strategies for bivalent ligands targeting GPCRs. ChemMedChem 2011;6:963–74.
[13] Huang St B, Onge CM, Ma H, Zhang Y. Design of bivalent ligands targeting putative GPCR dimers. Drug Discov Today 2021;26:189–99.
[14] Cordomí A, Navarro G, Pardo L, Franco R. Chapter 7 - Structure of G-protein-coupled receptor heteromers. In: Jastrzebska B, Park PS-H, editors. GPCRs. Academic Press; 2020. p. 109–19.
[15] Kaczor AA, Guixà-González R, Carrió P, Poso A, Dove S, Pastor M, et al. Multi-component protein - protein docking based protocol with external scoring for modeling dimers of g protein-coupled receptors. Mol Inf 2015;34:246–55.
[16] Guo W, Shi L, Javitch JA. The fourth transmembrane segment forms the interface of the dopamine D2 receptor homodimer. J Biol Chem 2003;278:4385–8.
[17] Guo W, Shi L, Filizola M, Weinstein H, Javitch JA. Crosstalk in G protein-coupled receptors: changes at the transmembrane homodimer interface determine activation. Proc Natl Acad Sci USA 2005;102:17495–500.
[18] Guo W, Urizar E, Kralikova M, Mobarec JC, Shi L, Filizola M, et al. Dopamine D2 receptors form higher order oligomers at physiological expression levels. EMBO J 2008;27:2293–304.
[19] Lee SP, O'Dowd BF, Rajaram RD, Nguyen T, George SR. D2 dopamine receptor homodimerization is mediated by multiple sites of interaction, including an intermolecular interaction involving transmembrane domain 4. Biochemistry 2003;42:11023–31.
[20] Jiang L-H. Cysteine-based cross-linking approach to study inter-domain interactions in ion channels. Methods Mol Biol 2013;998:267–76.
[21] Cottet M, Faklaris O, Maurel D, Scholler P, Doumazane E, Trinquet E, et al. BRET and Time-resolved FRET strategy to study GPCR oligomerization: from cell lines toward native tissues. Front Endocrinol 2012;3:92.
[22] Chen J, Cai X, Yan M, Wang Z, Lv Z, Wang C. A method for identifying G protein-coupled receptor dimers and their interfaces. Biochim Biophys Acta Mol Cell Res 2021;1868:118887.
[23] Wouters E, Marín AR, Dalton JAR, Giraldo J, Stove C. Distinct dopamine D_2 receptor antagonists differentially impact D_2 receptor oligomerization. Int J Mol Sci 2019:20. https://doi.org/10.3390/ijms20071686.

[24] Ng GY, O'Dowd BF, Lee SP, Chung HT, Brann MR, Seeman P, et al. Dopamine D2 receptor dimers and receptor-blocking peptides. Biochem Biophys Res Commun 1996;227:200–4.

[25] Beaulieu J-M, Espinoza S, Gainetdinov RR. Dopamine receptors - IUPHAR Review 13. Br J Pharm 2015;172:1–23.

[26] Borroto-Escuela DO, Brito I, Romero-Fernandez W, Di Palma M, Oflijan J, Skieterska K, et al. The G protein-coupled receptor heterodimer network (GPCR-HetNet) and its hub components. Int J Mol Sci 2014;15:8570–90.

[27] Kaczor AA, Jörg M, Capuano B. The dopamine D2 receptor dimer and its interaction with homobivalent antagonists: homology modeling, docking and molecular dynamics. J Mol Model 2016;22:203.

[28] Rangel-Barajas C, Coronel I, Florán B. Dopamine Receptors and Neurodegeneration. Aging Dis 2015;6:349–68.

[29] Blagotinšek Cokan K, Mavri M, Rutland CS, Glišić S, Senćanski M, Vrecl M, et al. Critical impact of different conserved endoplasmic retention motifs and dopamine receptor interacting proteins (DRIPs) on intracellular localization and trafficking of the D2 dopamine receptor (D2-R) isoforms. Biomolecules 2020:10. https://doi.org/10.3390/biom10101355.

[30] Kebabian JW. Multiple classes of dopamine receptors in mammalian central nervous system: the involvement of dopamine-sensitive adenylyl cyclase. Life Sci 1978;23:479–83.

[31] Andersen PH, Gingrich JA, Bates MD, Dearry A, Falardeau P, Senogles SE, et al. Dopamine receptor subtypes: beyond the D1/D2 classification. Trends Pharm Sci 1990;11:231–6.

[32] Carli M, Kolachalam S, Aringhieri S, Rossi M, Giovannini L, Maggio R, et al. Dopamine D2 receptors dimers: how can we pharmacologically target them? Curr Neuropharmacol 2018;16:222–30.

[33] Fiorentini C, Busi C, Spano P, Missale C. Dimerization of dopamine D1 and D3 receptors in the regulation of striatal function. Curr Opin Pharm 2010;10:87–92.

[34] Błasiak E, Łukasiewicz S, Szafran-Pilch K, Dziedzicka-Wasylewska M. Genetic variants of dopamine D2 receptor impact heterodimerization with dopamine D1 receptor. Pharm Rep 2017;69:235–41.

[35] Scarselli M, Novi F, Schallmach E, Lin R, Baragli A, Colzi A, et al. D2/D3 dopamine receptor heterodimers exhibit unique functional properties. J Biol Chem 2001;276:30308–14.

[36] Karpa KD, Lin R, Kabbani N, Levenson R. The dopamine D3 receptor interacts with itself and the truncated D3 splice variant d3nf: D3-D3nf interaction causes mislocalization of D3 receptors. Mol Pharm 2000;58:677–83.

[37] O'Dowd BF, Nguyen T, Ji X, George SR. D5 dopamine receptor carboxyl tail involved in D5-D2 heteromer formation. Biochem Biophys Res Commun 2013;431:586–9.

[38] Van Craenenbroeck K, Borroto-Escuela DO, Skieterska K, Duchou J, Romero-Fernandez W, Fuxe K. Role of dimerization in dopamine D(4) receptor biogenesis. Curr Protein Pept Sci 2014;15:659–65.

[39] Martel JC, Gatti, McArthur S. Dopamine receptor subtypes, physiology and pharmacology: new ligands and concepts in schizophrenia. Front Pharm 2020;11:1003.

[40] Wang M, Pei L, Fletcher PJ, Kapur S, Seeman P, Liu F. Schizophrenia, amphetamine-induced sensitized state and acute amphetamine exposure all show a common alteration: increased dopamine D2 receptor dimerization. Mol Brain 2010;3:25.

[41] Bagalkot TR, Jin H-M, Prabhu VV, Muna SS, Cui Y, Yadav BK, et al. Chronic social defeat stress increases dopamine D2 receptor dimerization in the prefrontal cortex of adult mice. Neuroscience 2015;311:444–52.

[42] Congreve M, de Graaf C, Swain NA, Tate CG. Impact of GPCR structures on drug discovery. Cell 2020;181:81–91.

[43] Borroto-Escuela DO, Rodriguez D, Romero-Fernandez W, Kapla J, Jaiteh M, Ranganathan A, et al. Mapping the Interface of a GPCR Dimer: A Structural Model of the A2A Adenosine and D2 Dopamine Receptor Heteromer. Front Pharm 2018;9:829.

[44] Mansoor S, Kayık G, Durdagi S, Sensoy O. Mechanistic insight into the impact of a bivalent ligand on the structure and dynamics of a GPCR oligomer. Comput Struct Biotechnol J 2022;20:925–36.

[45] Simpson LM, Taddese B, Wall ID, Reynolds CA. Bioinformatics and molecular modelling approaches to GPCR oligomerization. Curr Opin Pharm 2010;10:30–7.

[46] Armstrong D, Strange PG. Dopamine D2 receptor dimer formation: evidence from ligand binding. J Biol Chem 2001;276:22621–9.

[47] Xue L, Rovira X, Scholler P, Zhao H, Liu J, Pin J-P, et al. Major ligand-induced rearrangement of the heptahelical domain interface in a GPCR dimer. Nat Chem Biol 2015;11:134–40.

[48] Marsango S, Caltabiano G, Pou C, Varela Liste MJ, Milligan G. Analysis of Human Dopamine D3 Receptor Quaternary Structure. J Biol Chem 2015;290:15146–62.

[49] Wang S, Che T, Levit A, Shoichet BK, Wacker D, Roth BL. Structure of the D2 dopamine receptor bound to the atypical antipsychotic drug risperidone. Nature 2018;555:269–73.

[50] Yin J, Chen K-YM, Clark MJ, Hijazi M, Kumari P, Bai X-C, et al. Structure of a D2 dopamine receptor-G-protein complex in a lipid membrane. Nature 2020;584:125–9.

[51] Webb B, Sali A. Comparative Protein Structure Modeling Using MODELLER. Curr Protoc Bioinforma 2016;54:5.6.1–5.6.37.

[52] Preto AJ, Barreto CAV, Baptista SJ, Almeida JG, de, Lemos A, Melo A, et al. Understanding the binding specificity of G-protein coupled receptors toward G-proteins and arrestins: application to the dopamine receptor family. J Chem Inf Model 2020;60:3969–84.

[53] Rasmussen SGF, DeVree BT, Zou Y, Kruse AC, Chung KY, Kobilka TS, et al. Crystal structure of the β2 adrenergic receptor-Gs protein complex. Nature 2011;477:549–55.

[54] Staus DP, Hu H, Robertson MJ, Kleinhenz ALW, Wingler LM, Capel WD, et al. Structure of the M2 muscarinic receptor-β-arrestin complex in a lipid nanodisc. Nature 2020;579:297–302.

[55] Humphrey W, Dalke A, Schulten K. VMD: visual molecular dynamics. J Mol Graph 1996;14(33–8):27–8.

[56] Kaufmann KW, Lemmon GH, Deluca SL, Sheehan JH, Meiler J. Practically useful: what the Rosetta protein modeling suite can do for you. Biochemistry 2010;49:2987–98.

[57] Elez K, Bonvin AMJJ, Vangone A. Distinguishing crystallographic from biological interfaces in protein complexes: role of intermolecular contacts and energetics for classification. BMC Bioinforma 2018;19:438.

[58] Jiménez-García B, Elez K, Koukos PI, Bonvin AM, Vangone A. PRODIGY-crystal: a web-tool for classification of biological interfaces in protein complexes. Bioinformatics 2019;35:4821–3.

[59] Xue LC, Rodrigues JP, Kastritis PL, Bonvin AM, Vangone A. PRODIGY: a web server for predicting the binding affinity of protein-protein complexes. Bioinformatics 2016;32:3676–8.

[60] Prodigy Webserver. [cited 7 Jul 2022]. Available: ⟨https://bianca.science.uu.nl/prodigy/⟩.

[61] Vangone A, Bonvin AM. Contacts-based prediction of binding affinity in protein-protein complexes. Elife 2015;4:e07454.

[62] Ballesteros JA, Weinstein H. [19] Integrated methods for the construction of three-dimensional models and computational probing of structure-function relations in G protein-coupled receptors. In: Sealfon SC, editor. Methods in Neurosciences. Academic Press; 1995. p. 366–428.

[63] Moreira IS. Structural features of the G-protein/GPCR interactions. Biochim Biophys Acta 2014;1840:16–33.

[64] Lomize MA, Pogozheva ID, Joo H, Mosberg HI, Lomize AL. OPM database and PPM web server: resources for positioning of proteins in membranes. Nucleic Acids Res 2012;40:D370–6.

[65] Jo S, Kim T, Iyer VG, Im W. CHARMM-GUI: a web-based graphical user interface for CHARMM. J Comput Chem 2008;29:1859–65.

[66] Lee J, Cheng X, Jo S, MacKerell AD, Klauda JB, Im W. CHARMM-GUI input generator for NAMD, gromacs, amber, openmm, and CHARMM/OpenMM simulations using the CHARMM36 additive force field. Biophys J 2016:641a. https://doi.org/10.1016/j.bpj.2015.11.3431.

[67] Wu EL, Cheng X, Jo S, Rui H, Song KC, Dávila-Contreras EM, et al. CHARMM-GUI membrane builder toward realistic biological membrane simulations. J Comput Chem 2014;35:1997–2004.

[68] Jo S, Cheng X, Islam SM, Huang L, Rui H, Zhu A, et al. Chapter eight - CHARMM-GUI PDB manipulator for advanced modeling and simulations of proteins containing nonstandard residues. In: Karabencheva-Christova T, editor. Advances in Protein Chemistry and Structural Biology. Academic Press; 2014. p. 235–65.

[69] Ranganathan A, Dror RO, Carlsson J. Insights into the role of $Asp79^{2.50}$ in β_2 adrenergic receptor activation from molecular dynamics simulations. Biochemistry 2014:7283–96. https://doi.org/10.1021/bi5008723.

[70] Fleetwood O, Matricon P, Carlsson J, Delemotte L. Energy landscapes reveal agonist control of G protein-coupled receptor activation via microswitches. Biochemistry 2020;59:880–91.

[71] Katritch V, Fenalti G, Abola EE, Roth BL, Cherezov V, Stevens RC. Allosteric sodium in class A GPCR signaling. Trends Biochem Sci 2014:233–44. https://doi.org/10.1016/j.tibs.2014.03.002.

[72] Liu W, Chun E, Thompson AA, Chubukov P, Xu F, Katritch V, et al. Structural basis for allosteric regulation of GPCRs by sodium ions. Science 2012;337:232–6.

[73] Vickery ON, Carvalheda CA, Zaidi SA, Pisliakov AV, Katritch V, Zachariae U. Intracellular Transfer of Na+ in an Active-State G-Protein-Coupled Receptor. Structure 2018;26:171–80. e2.

[74] Kim S, Lee J, Jo S, Brooks 3rd CL, Lee HS, Im W. CHARMM-GUI ligand reader and modeler for CHARMM force field generation of small molecules. J Comput Chem 2017;38:1879–86.

[75] Abraham MJ, Murtola T, Schulz R, Páll S, Smith JC, Hess B, et al. GROMACS: High performance molecular simulations through multi-level parallelism from laptops to supercomputers. SoftwareX 2015;1–2:19–25.

[76] Brooks BR, Brooks CL 3rd, Mackerell ADJr, Nilsson L, Petrella RJ, Roux B, et al. CHARMM: the biomolecular simulation program. J Comput Chem 2009;30:1545–614.

[77] Lindahl E, Hess B, van der Spoel D. GROMACS 3.0: a package for molecular simulation and trajectory analysis. Mol Model Annu 2001;7:306–17.

[78] Bussi G, Donadio D, Parrinello M. Canonical sampling through velocity rescaling. J Chem Phys 2007;126:014101.

[79] Nosé S, Klein ML. Constant pressure molecular dynamics for molecular systems. Mol Phys 1983;50:1055–76.

[80] Parrinello M, Rahman A. Polymorphic transitions in single crystals: a new molecular dynamics method. J Appl Phys 1981;52:7182–90.

[81] Darden T, York D, Pedersen L. Particle mesh Ewald: An N·log(N) method for Ewald sums in large systems. J Chem Phys 1993;98:10089–92.

[82] Essmann U, Perera L, Berkowitz ML, Darden T, Lee H, Pedersen LG. A smooth particle mesh Ewald method. J Chem Phys 1995;103:8577–93.

[83] Páll S, Hess B. A flexible algorithm for calculating pair interactions on SIMD architectures. Comput Phys Commun 2013;184:2641–50.

[84] Hess B. P-LINCS: a parallel linear constraint solver for molecular simulation. J Chem Theory Comput 2008;4:116–22.

[85] Luenberger D.G., Ye Y. Linear and Nonlinear Programming. Springer International Publishing;
[86] Bueschbell B, Barreto CAV, Preto AJ, Schiedel AC, Moreira IS. A complete assessment of dopamine receptor- ligand interactions through computational methods. Molecules 2019:24. https://doi.org/10.3390/molecules24071196.
[87] Zhou Q, Yang D, Wu M, Guo Y, Guo W, Zhong L, et al. Common activation mechanism of class A GPCRs. Elife 2019:8. https://doi.org/10.7554/eLife.50279.
[88] Cherezov V, Rosenbaum DM, Hanson MA, Rasmussen SGF, Thian FS, Kobilka TS, et al. High-resolution crystal structure of an engineered human beta2-adrenergic G protein-coupled receptor. Science 2007;318:1258–65.
[89] Rasmussen SGF, Choi H-J, Fung JJ, Pardon E, Casarosa P, Chae PS, et al. Structure of a nanobody-stabilized active state of the β(2) adrenoceptor. Nature 2011;469:175–80.
[90] Kaczor AA, Bartuzi D, Stępniewski TM, Matosiuk D, Selent J. Protein–protein docking in drug design and discovery. In: Gore M, Jagtap UB, editors. Computational Drug Discovery and Design. New York, NY. New York: Springer; 2018. p. 285–305.
[91] Karaca E, Prévost C, Sacquin-Mora S. Modeling the dynamics of protein-protein interfaces, how and why? Molecules 2022:27. https://doi.org/10.3390/molecules27061841.
[92] Erol I, Cosut B, Durdagi S. Toward understanding the impact of dimerization interfaces in angiotensin II Type 1 receptor. J Chem Inf Model 2019;59:4314–27.
[93] Wang L, Yuan Y, Chen X, Chen J, Guo Y, Li M, et al. Probing the cooperative mechanism of the μ–δ opioid receptor heterodimer by multiscale simulation. Phys Chem Chem Phys 2018;20:29969–82.
[94] Kasai RS, Ito SV, Awane RM, Fujiwara TK, Kusumi A. The Class-A GPCR Dopamine D2 Receptor Forms Transient Dimers Stabilized by Agonists: Detection by Single-Molecule Tracking. Cell Biochem Biophys 2018;76:29–37.
[95] Han Y, Moreira IS, Urizar E, Weinstein H, Javitch JA. Allosteric communication between protomers of dopamine class A GPCR dimers modulates activation. Nat Chem Biol 2009;5:688–95.
[96] Leioatts N, Suresh P, Romo TD, Grossfield A. Structure-based simulations reveal concerted dynamics of GPCR activation. Proteins 2014;82:2538–51.
[97] Ballesteros, Jensen, Liapakis. Activation of the β2-adrenergic receptor involves disruption of an ionic lock between the cytoplasmic ends of transmembrane segments 3 and 6. Boll Soc Ital Biol Sper. Available: https://www.jbc.org/article/S0021–9258(20)80383–4/abstract.
[98] Vogel R, Mahalingam M, Lüdeke S, Huber T, Siebert F, Sakmar TP. Functional role of the "ionic lock"–an interhelical hydrogen-bond network in family A heptahelical receptors. J Mol Biol 2008;380:648–55.
[99] Han X, Feng Y, Chen X, Gerard C, Boisvert WA. Characterization of G protein coupling mediated by the conserved D134(3.49) of DRY motif, M241(6.34), and F251(6.44) residues on human CXCR1. FEBS Open Bio 2015;5:182–90.
[100] Yuan S, Filipek S, Palczewski K, Vogel H. Activation of G-protein-coupled receptors correlates with the formation of a continuous internal water pathway. Nat Commun 2014;5:4733.
[101] Latorraca NR, Venkatakrishnan AJ, Dror RO. GPCR dynamics: structures in motion. Chem Rev 2017;117:139–55.
[102] Fleetwood O, Carlsson J, Delemotte L. Identification of ligand-specific G protein-coupled receptor states and prediction of downstream efficacy via data-driven modeling. Elife 2021:10. https://doi.org/10.7554/eLife.60715.
[103] Lu S, He X, Yang Z, Chai Z, Zhou S, Wang J, et al. Activation pathway of a G protein-coupled receptor uncovers conformational intermediates as targets for allosteric drug design. Nat Commun 2021. https://doi.org/10.1038/s41467-021-25020-9.
[104] Floresca CZ, Schetz JA. Dopamine receptor microdomains involved in molecular recognition and the regulation of drug affinity and function. J Recept Signal Transduct Res 2004;24:207–39.
[105] Zou R, Wang X, Li S, Chan HCS, Vogel H, Yuan S. The role of metal ions in G protein-coupled receptor signalling and drug discovery. Wiley Inter Rev Comput Mol Sci 2022:12. https://doi.org/10.1002/wcms.1565.
[106] Gutiérrez-de-Terán H, Massink A, Rodríguez D, Liu W, Han GW, Joseph JS, et al. The role of a sodium ion binding site in the allosteric modulation of the A2A adenosine G protein-coupled receptor. Structure 2013;21:2175–85.
[107] Miller-Gallacher JL, Nehmé R, Warne T, Edwards PC, Schertler GFX, Leslie AGW, et al. The 2.1 Å resolution structure of cyanopindolol-bound β1-adrenoceptor identifies an intramembrane Na+ ion that stabilises the ligand-free receptor. PLoS One 2014;9:e92727.
[108] Tehan BG, Bortolato A, Blaney FE, Weir MP, Mason JS. Unifying family A GPCR theories of activation. Pharm Ther 2014;143:51–60.
[109] Dror RO, Arlow DH, Maragakis P, Mildorf TJ, Pan AC, Xu H, et al. Activation mechanism of the β2-adrenergic receptor. Proc Natl Acad Sci USA 2011;108:18684–9.
[110] Gorinski N, Kowalsman N, Renner U, Wirth A, Reinartz MT, Seifert R, et al. Computational and Experimental Analysis of the Transmembrane Domain 4/5 Dimerization Interface of the Serotonin 5-HT1A Receptor. Mol Pharm 2012;82:448–63.
[111] Prasanna X, Sengupta D, Chattopadhyay A. Cholesterol-dependent conformational plasticity in GPCR Dimers. Sci Rep 2016;6:31858.
[112] Carrillo JJ, López-Giménez JF, Milligan G. Multiple interactions between transmembrane helices generate the oligomeric α_{1b}-adrenoceptor. Mol Pharmacol 2004:1123–37. https://doi.org/10.1124/mol.104.001586.
[113] Lopez-Gimenez JF, Canals M, Pediani JD, Milligan G. The α1b-adrenoceptor exists as a higher-order oligomer: effective oligomerization is required for receptor maturation, surface delivery, and function. Mol Pharm 2007;71:1015–29.
[114] Mancia F, Assur Z, Herman AG, Siegel R, Hendrickson WA. Ligand sensitivity in dimeric associations of the serotonin 5HT2c receptor. EMBO Rep 2008;9:363–9.
[115] Huang J, Chen S, Zhang JJ, Huang X-Y. Crystal structure of oligomeric β1-adrenergic G protein–coupled receptors in ligand-free basal state. Nat Struct Mol Biol 2013;20:419–25.
[116] Filizola M. Increasingly accurate dynamic molecular models of G-protein coupled receptor oligomers: Panacea or Pandora's box for novel drug discovery? Life Sci 2010;86:590–7.
[117] Perreault ML, Hasbi A, O'Dowd BF, George SR. Heteromeric dopamine receptor signaling complexes: emerging neurobiology and disease relevance. Neuropsychopharmacology 2014;39:156–68.
[118] González-Maeso J, Ang RL, Yuen T, Chan P, Weisstaub NV, López-Giménez JF, et al. Identification of a serotonin/glutamate receptor complex implicated in psychosis. Nature 2008;452:93–7.
[119] Liu J, Tang H, Xu C, Zhou S, Zhu X, Li Y, et al. Biased signaling due to oligomerization of the G protein-coupled platelet-activating factor receptor. Nat Commun 2022;13:6365.
[120] Wu B, Chien EYT, Mol CD, Fenalti G, Liu W, Katritch V, et al. Structures of the CXCR4 chemokine GPCR with small-molecule and cyclic peptide antagonists. Science 2010;330:1066–71.
[121] Guidolin D, Marcoli M, Tortorella C, Maura G, Agnati LF. G protein-coupled receptor-receptor interactions give integrative dynamics to intercellular communication. Rev Neurosci 2018;29:703–26.
[122] Liu F, Wan Q, Pristupa ZB, Yu XM, Wang YT, Niznik HB. Direct protein-protein coupling enables cross-talk between dopamine D5 and gamma-aminobutyric acid A receptors. Nature 2000;403:274–80.
[123] Dijkman PM, Castell OK, Goddard AD, Munoz-Garcia JC, de Graaf C, Wallace MI, et al. Dynamic tuneable G protein-coupled receptor monomer-dimer populations. Nat Commun 2018;9:1710.
[124] Cordomí A, Navarro G, Aymerich MS, Franco R. Structures for G-protein-coupled receptor tetramers in complex with G proteins. Trends Biochem Sci 2015;40:548–51.
[125] Vafabakhsh R, Levitz J, Isacoff EY. Conformational dynamics of a class C G-protein-coupled receptor. Nature 2015;524:497–501.
[126] Pulido D, Casadó-Anguera V, Pérez-Benito L, Moreno E, Cordomí A, López L, et al. Design of a true bivalent ligand with picomolar binding affinity for a G protein-coupled receptor homodimer. J Med Chem 2018;61:9335–46.
[127] Gahbauer S, Böckmann RA. Membrane-mediated oligomerization of g protein coupled receptors and its implications for GPCR function. Front Physiol 2016;7:494.
[128] Gurevich VV, Gurevich EV. How and why do GPCRs dimerize? Trends Pharm Sci 2008;29:234–40.
[129] Jackson SN, Wang H-YJ, Yergey A, Woods AS. Phosphate stabilization of intermolecular interactions. J Proteome Res 2006;5:122–6.
[130] Woods AS, Ferré S. Amazing stability of the arginine-phosphate electrostatic interaction. J Proteome Res 2005;4:1397–402.
[131] Johnston JM, Aburi M, Provasi D, Bortolato A, Urizar E, Lambert NA, et al. Making structural sense of dimerization interfaces of delta opioid receptor homodimers. Biochemistry 2011;50:1682–90.
[132] Teng X, Chen S, Wang Q, Chen Z, Wang X, Huang N, et al. Structural insights into G protein activation by D1 dopamine receptor. Sci Adv 2022;8:eabo4158.
[133] Borroto-Escuela DO, Romero-Fernandez W, Tarakanov AO, Gómez-Soler M, Corrales F, Marcellino D, et al. Characterization of the A2AR–D2R interface: Focus on the role of the C-terminal tail and the transmembrane helices. Biochem Biophys Res Commun 2010;402:801–7.
[134] George SR, Kern A, Smith RG, Franco R. Dopamine receptor heteromeric complexes and their emerging functions. Prog Brain Res 2014;211:183–200.
[135] O'Dowd BF, Ji X, Nguyen T, George SR. Two amino acids in each of D1 and D2 dopamine receptor cytoplasmic regions are involved in D1–D2 heteromer formation. Biochem Biophys Res Commun 2012;417:23–8.
[136] Perreault ML, Hasbi A, Alijaniaram M, Fan T, Varghese G, Fletcher PJ, et al. The dopamine D1-D2 receptor heteromer localizes in dynorphin/enkephalin neurons. J Biol Chem 2010:36625–34. https://doi.org/10.1074/jbc.m110.159954.
[137] Damian M, Martin A, Mesnier D, Pin J-P, Banères J-L. Asymmetric conformational changes in a GPCR dimer controlled by G-proteins. EMBO J 2006:5693–702. https://doi.org/10.1038/sj.emboj.7601449.
[138] Brock C, Oueslati N, Soler S, Boudier L, Rondard P, Pin J-P. Activation of a dimeric metabotropic glutamate receptor by intersubunit rearrangement. J Biol Chem 2007;282:33000–8.
[139] Guitart X, Navarro G, Moreno E, Yano H, Cai N-S, Sánchez-Soto M, et al. Functional selectivity of allosteric interactions within G protein-coupled receptor oligomers: the dopamine D1-D3 receptor heterotetramer. Mol Pharm 2014;86:417–29.
[140] Guitart X, Moreno E, Rea W, Sánchez-Soto M, Cai N-S, Quiroz C, et al. Biased G Protein-Independent Signaling of Dopamine D1-D3 Receptor Heteromers in the Nucleus Accumbens. Mol Neurobiol 2019;56:6756–69.
[141] Maggio R, Millan MJ. Dopamine D2–D3 receptor heteromers: pharmacological properties and therapeutic significance. Curr Opin Pharm 2010;10:100–7.
[142] Maggio R, Scarselli M, Novi F, Millan MJ, Corsini GU. Potent activation of dopamine D3/D2 heterodimers by the antiparkinsonian agents, S32504, pramipexole and ropinirole. J Neurochem 2003;87:631–41.
[143] Caniceiro AB, Bueschbell B, Barreto CAV, Preto AJ, Moreira IS. MUG: a mutation overview of GPCR subfamily A17 receptors. Comput Struct Biotechnol J 2022. https://doi.org/10.1016/j.csbj.2022.12.031.
[144] Zhang R, Li D, Mao H, Wei X, Xu M, Zhang S, et al. Disruption of 5-hydroxytryptamine 1A receptor and orexin receptor 1 heterodimer formation affects novel

G protein-dependent signaling pathways and has antidepressant effects in vivo. Transl Psychiatry 2022;12:122.
[145] Lira SS, Ahammad I. A comprehensive in silico investigation into the nsSNPs of Drd2 gene predicts significant functional consequences in dopamine signaling and pharmacotherapy. Sci Rep 2021;11:23212.
[146] Mondal S, Johnston JM, Wang H, Khelashvili G, Filizola M, Weinstein H. Membrane driven spatial organization of GPCRs. Sci Rep 2013;3:2909.
[147] Sankararamakrishnan R, Weinstein H. Positioning and stabilization of dynorphin peptides in membrane bilayers: the mechanistic role of aromatic and basic residues revealed from comparative MD simulations. J Phys Chem B 2002: 209–18. https://doi.org/10.1021/jp012174o.
[148] Ma X, Hu Y, Batebi H, Heng J, Xu J, Liu X, et al. Analysis of β2AR-Gs and β2AR-Gi complex formation by NMR spectroscopy. Proc Natl Acad Sci USA 2020;117: 23096–105.
[149] Wang X, Cheng X, Zhao L, Wang Y, Ye C, Zou X, et al. Molecular insights into differentiated ligand recognition of the human parathyroid hormone receptor 2. Proc Natl Acad Sci Usa 2021:118. https://doi.org/10.1073/pnas.2101279118.
[150] Ma X, Segura MA, Zarzycka B, Vischer HF, Leurs R. Analysis of missense variants in the human histamine receptor family reveals increased constitutive activity of E4106.30×30K variant in the histamine H1 receptor. Int J Mol Sci 2021;22. https://doi.org/10.3390/ijms22073702.
[151] Cai X, Wang D, Zhang R, Chen Y, Chen J. The transmembrane domains of GPCR dimers as targets for drug development. Drug Discov Today 2022;28:103419.
[152] Lipiński PFJ, Jarończyk M, Dobrowolski JC, Sadlej J. Molecular dynamics of fentanyl bound to μ-opioid receptor. J Mol Model 2019;25:144.
[153] Zou Y, Ewalt J, Ng H-L. Recent insights from molecular dynamics simulations for G protein-coupled receptor drug discovery. Int J Mol Sci 2019:20. https://doi.org/10.3390/ijms20174237.
[154] Wu Y, Li X, Hua T, Liu Z-J, Liu H, Zhao S. MD simulations revealing special activation mechanism of cannabinoid receptor 1. Front Mol Biosci 2022;9: 860035.